



## AN ABSTRACT OF THE DISSERTATION OF

Spencer Liverman for the degree of Doctor of Philosophy in Electrical and Computer Engineering presented on February 13, 2019.

Title: Design and Analysis of Free-space Optical Communications Systems for Next Generation Short-range Wireless Networks

Abstract approved:

---

Alan X. Wang

This dissertation focuses on indoor free-space optical communications systems for use in short range wireless networks. We propose that current radio frequency wireless links be augmented or replaced with optical frequency links due to overcrowding in the radio frequency spectrum. Optical frequencies contain hundreds of terahertz of unregulated bandwidth and offer a physical layer of protection due to the inherently line-of-sight nature of near infrared light. We first present a hybrid optical and radio frequency link based on inexpensive LEDs in which a downlink is established optically, while the uplink is routed through preexisting radio frequency channels. Second, an all optical dual channel laser-based communication system is implemented consisting of a medium bandwidth wide-angle optical femtocell and a high-speed line-of-sight optical attocell. This approach balances the diverse needs of end users by providing links optimized for both mobility and bandwidth. Lastly, we demonstrate a high-power vertical cavity surface emitting laser (VCSEL) array transmitter for use in optical femtocells. A complimentary design for a distributed current laser driver is also presented.

©Copyright by Spencer Liverman  
February 13, 2019  
All Rights Reserved

Design and Analysis of Free-space Optical Communications Systems for Next  
Generation Short-range Wireless Networks

by  
Spencer Liverman

A DISSERTATION

submitted to

Oregon State University

in partial fulfillment of  
the requirements for the  
degree of

Doctor of Philosophy

Presented February 13, 2019  
Commencement June 2019

Doctor of Philosophy dissertation of Spencer Liverman presented on February 13, 2019

APPROVED:

---

Major Professor, representing Electrical and Computer Engineering

---

Head of the School of Electrical Engineering and Computer Science

---

Dean of the Graduate School

I understand that my dissertation will become part of the permanent collection of Oregon State University libraries. My signature below authorizes release of my dissertation to any reader upon request.

---

Spencer Liverman, Author

## ACKNOWLEDGEMENTS

I would like to express my genuine gratitude toward my advisor Professor Alan X. Wang for his guidance and mentorship throughout my graduate school education. I greatly appreciate the opportunities that he has afforded me and the time that he has invested in my academic development. My appreciation also extends to Professor Thinh Nguyen and Professor Arun Natarajan who closely collaborated with me on my various research projects. I am also very thankful to Professor Lizhong Chen, Professor Yun-Shik Lee, and Professor Matthew Johnston for serving on my graduate committee.

I would also like to thank all my current and former laboratory colleagues for their support and friendship: Hayden Bialek, Qiwei Wang, Yu-Jung Chu, Anindita Borah, Songtao Wang, and Siyuan Chen among several others.

I extend a very special thank you to Martin Now, whose literary skills have saved my writing more than once. This document would not be what it is without his invaluable contribution.

Lastly, I would like to acknowledge with gratitude, the love and support I have received from my family. The completion of my Ph.D. degree would not have been possible without them.

## TABLE OF CONTENTS

	<u>Page</u>
1 Introduction .....	1
1.1 Optical Communication Components and Methods .....	3
1.1.1 External Modulation Method .....	4
1.1.2 Direct-drive Modulation Method .....	6
1.2 Transmitter Light Source Selection .....	8
1.2.1 LED Transmitters .....	9
1.2.2 FP Laser Diode Transmitters .....	11
1.2.3 VCSEL Diode Transmitters .....	12
1.3 Optical Receiver Design .....	14
1.4 Dissertation Organization .....	16
2 Hybrid Free-space Optical and RF Communication Networks .....	18
2.1 Background .....	20
2.2 WiFO System .....	24
2.2.1 Transmitter .....	26
2.2.2 Receiver .....	30
2.2.3 Network Protocol .....	35
2.3 System Evaluation .....	42
2.3.1 Bit Error Rate without FEC .....	44
2.3.2 Bit Error Rate with FEC – Fixed Lateral Offset .....	45

## TABLE OF CONTENTS (Continued)

	<u>Page</u>
2.3.3 Bit Error Rate with FEC – Fixed Vertical Offset.....	45
2.3.4 Angular Dependence.....	46
2.3.5 Bit Error Rate as a Function of Data Rate.....	46
2.3.6 Ambient Light Effect.....	48
2.3.7 Evaluation of FSO and WiFi Channel Throughputs.....	48
2.3.8 Transition Time Analysis.....	51
2.4 Summary.....	52
3 Dual-channel Femtocell and Attocell Optical Links for Indoor Wireless Networks.....	54
3.1 Background.....	55
3.2 Dual Channel Optical Link.....	58
3.2.1 Femtocell Design.....	62
3.2.2 Attocell Design.....	64
3.2.3 Optical Receiver Design.....	67
3.3 Dual Channel Link Evaluation.....	71
3.3.1 Femtocell Performance Evaluation.....	73
3.3.2 Attocell Performance Evaluation.....	75
3.3.3 Dual Channel System Evaluation.....	78
3.4 Summary.....	80

## TABLE OF CONTENTS (Continued)

	<u>Page</u>
4 High-power High-speed VCSEL Array Centric PSO Transmitter and Laser Driver Design .....	81
4.1 Background .....	84
4.2 VCSEL Array FSO Link Design .....	87
4.2.1 VCSEL Array Transmitter .....	88
4.2.2 FSO Link Receiver .....	96
4.3 FSO Link Evaluation .....	98
4.3.1 Lateral Motion Tolerance .....	101
4.3.2 Angular Motion Tolerance .....	102
4.3.3 Data Throughput Evaluation .....	104
4.3.4 PAM4 Modulation Symbols .....	106
4.4 Summary .....	108
5 Conclusions .....	109
References .....	113

## LIST OF FIGURES

<u>Figure</u>	<u>Page</u>
Figure 2.1: WiFO system – (a) high-level system block diagram, (b) FSO experimental setup with zoomed views of the optical transmitter and receiver.....	26
Figure 2.2: Free-space optical transmitter – (a) transmitter schematic, (b) improvement of the optical fall time with sweep out transistors included, (c) normalized frequency response.....	29
Figure 2.3: Free-space optical receiver – (a) receiver block diagram, (b) photodiode angular dependence, (c) photocurrent generated at the receiver, (d) eye diagram showing a 50 Mb/s received signal sent over a distance of one meter before the signal is saturated by the limiting amplifier.....	33
Figure 2.4: AP application – (a) application diagram detailing the main threads, user, and FSO cone table formats, (b) diagram showing data process sub-threads, (c) formats of packets, which keep the user and FSO cone tables updated.....	41
Figure 2.5: FSO channel spatial parameters.....	42
Figure 2.6: Bit error-rate measurements taken at 25 Mb/s – (a) un-coded BER as a function of vertical and lateral distance, (b) Reed-Solomon coded BER with fixed .1 m lateral offset, (c) Reed-Solomon coded BER with fixed .3 m lateral offset, (d) Reed-Solomon coded BER with fixed 2.1 m vertical offset, (e) Reed-Solomon coded BER with fixed 2.8 m vertical offset, (f) un-coded BER angular dependence.....	43
Figure 2.7: Data throughput analysis – (a) BER comparison at various data rates, (b) maximum achievable data rates given set BER requirements, (c) ambient light effect on BER.....	47
Figure 2.8: Throughput comparison between the FSO and WiFi channel.....	49
Figure 2.9: Roundtrip times in the FSO channel.....	50

## LIST OF FIGURES (Continued)

<u>Figure</u>	<u>Page</u>
Figure 3.1: Overlapping FSO femtocell and attocell profiles – (a) top view with honeycomb AP packing, (b) side view with design constraints shown.....	60
Figure 3.2: Laser driver schematic used for both the femtocell and attocell transmitters.....	63
Figure 3.3: FSO transmitter PCBs showing the femtocell and attocell transmitters mounted to a 3 m optical rail.....	66
Figure 3.4: Dual-channel FSO receiver – (a) schematic for both the femtocell and attocell receivers, (b) femtocell and attocell receivers mounted to the 50 cm lateral optical rail.....	69
Figure 3.5: FSO dual-channel test configuration – (a) diagram of relevant test parameters, (b) block diagram detailing the main components of the test setup, (c) experimental test setup with 3 m vertical optical rail and 50 cm lateral optical rail.....	71
Figure 3.6: Optical femtocell evaluation – (a) BER evaluation at various vertical and lateral distances, 100 Mb/s (b) BER evaluation at various vertical distances and incident angles, 100 Mb/s (c) BER evaluation at various vertical distances and bit rates.....	73
Figure 3.7: Optical attocell evaluation – (a) BER evaluation at various incident angles over a vertical distance of 3 m, 1 Gb/s (b) BER evaluation at various bit rates over a vertical distance of 3 m.....	77
Figure 3.8: Recovered eye diagrams for the femtocell (blue) and attocell (teal) links at data rates of 100 Mb/s and 1 Gb/s respectively over a distance of 3 m.....	79

## LIST OF FIGURES (Continued)

<u>Figure</u>	<u>Page</u>
Figure 4.1: 850 nm VCSEL array light source – (a) image of the 60-element VCSEL array device, (b) VCSEL IV curve showing various regions of operation.....	90
Figure 4.2: S11 simulations of E-pHEMT devices – (a) ATF-511P8, (b) ATF-531P8, (c) ATF-55143.....	93
Figure 4.3: VCSEL array transmitter – (a) schematic of distributed current VCSEL array driver, (b) fabricated transmitter PCB with and without a collimation lens mounted.....	95
Figure 4.4: High-sensitivity optical receiver – (a) block diagram detailing optical receiver data path, (b) optical receiver PCB shown with functional block on the front of the board and an APD mounted to the back of the board.....	97
Figure 4.5: FSO channel test configuration – (a) block diagram detailing the components used in the test configuration, (b) diagram showing the FSO test parameters, (c) a photo of the experimental setup showing the .5m optical rail mounted orthogonally to the 3 m optical rail.....	99
Figure 4.6: FSO system BER measurements collected at a distance of 3 m – (a) BER as a function of lateral motion, (b) BER as a function incident angle with respect to the optical receiver, (c) BER as a function of data throughput.....	100
Figure 4.7: Eye diagrams showing FSO signals recovered over a 3 m optical channel – (a) 1 Gb/s, (b) 1.25 Gb/s, (c) 1.45 Gb/s.....	105
Figure 4.8: Eye diagrams showing PAM4 signals recovered over a 3 m optical channel – (a) 1 Gb/s, (b) 2 Gb/s.....	107

## LIST OF TABLES

<u>Table</u>	<u>Page</u>
2.1 Transmitter Components.....	30
2.2 Receiver Components.....	34
2.3 Cone IDs and Users' Locations.....	40
2.4 Handoff Transition Times.....	52
3.1 Femtocell Transmitter Components.....	64
3.2 Attocell Transmitter Components.....	66
3.3 (a) Femtocell Receiver Components, (b) Attocell Receiver Components.....	70
4.1 E-pHEMT Device Summary.....	92
4.2 VCSEL Array Transmitter Components.....	96
4.3 Optical Receiver Components.....	98

## CHAPTER 1: INTRODUCTION

Optical communication systems have revolutionized the way in which information is created, transported, and recovered around the world. The versatility and bandwidth potential of these systems is unparalleled, with data throughputs increasing exponentially year after year. Although human beings have used light to communicate with one another for thousands of years, the technology that has enabled the rapid development of modern optical communication systems has only existed for a few decades. Advancements in the field of quantum physics led to the development of the first laser in 1960 by Theodore Maiman, and just two years later, the light emitting diode (LED) by Nick Holonyak. Together, these two discoveries would eventually be used to transform communication networks worldwide.

Optical communication systems can be fundamentally categorized as either guided-light systems or free-space optical (FSO) systems. Guided-light systems confine and direct light into a desired medium using the property of total internal reflection. If light travelling through a material with a high index of refraction reaches an interface with a material of a low index of refraction, the light is refracted. If the incident angle of that interaction exceeds the critical angle of the interface, the light is reflected back into the high-index material. This property is harnessed in optical fibers and waveguides to route light emitted from an LED or

laser to a desired location. Optical fibers, in particular, have been used to confine and direct light over hundreds of kilometers with minimal losses, enabling high-speed intercontinental communication links. However, guided-light systems require a physical connection between the ends of the communication link and are not appropriate for all applications.

FSO communication systems conduct light through an open medium with no physical connection between the transmitter and receiver. This allows FSO systems to be implemented in environments that would make the use of guided-light optical systems physically impossible or highly impractical. Specific examples include communication links between a satellite and the earth, between objects in space, and between locations on the ground where fiberoptic infrastructure does not exist.

Radio frequency (RF) communication links have been traditionally used in such circumstances; however, due to overcrowding in the RF spectrum, bandwidth is highly limited. RF transmissions are usually broadcast, which means that the available bandwidth must be divided between users. Optical communication links are inherently line-of-sight (LOS) and therefore do not require a division of spectral resources. Furthermore, interception of an optical transmission is impossible unless the intercepting receiver is in the direct path of the transmitting beam. This provides a layer of additional security to each transmission sent or received.

Recently, short-range FSO communication systems have been explored as a means of augmenting or replacing indoor wireless RF technologies, such as WiFi. Indoor optical links are a unique subset of FSO systems and present a unique set of design challenges. This dissertation will examine various indoor FSO communication technologies and test their effectiveness through the creation of prototype systems. However, before addressing the challenges inherent to designing these systems, it is necessary to establish foundational knowledge of the components and methods that will be used.

## **1.1 Free-space Optical Communication Components and Methods**

The first, most fundamental question that must be asked is how the transmitted light beam will be altered or modulated to send a message. All messaging systems must utilize a medium through which a message can be sent—in this case light—and then modulate that medium in some way to convey information.

Optical rays have been identified as a particularly attractive medium for the transfer of information because they travel at the speed of causality and have several properties that can be manipulated: amplitude, phase, and polarization. Optical rays are also electromagnetic waves that can propagate freely through a vacuum. Currently, the property of optical waves that is most commonly manipulated is amplitude. Due to the extremely high frequency of optical waves, manipulation of the phase is technically difficult, and the manipulation of polarization introduces

an otherwise avoidable dependence on the relative orientation between the transmitter and receiver. Therefore, the prototype systems presented in this body of work will operate exclusively on the principle of amplitude modulation.

### **1.1.1 External Modulation Method**

Optical amplitude modulators can be further categorized into external modulators and direct modulators. External modulators accept a continuous wave (CW) input beam of light and then either attenuate the beam or let the beam pass through unattenuated. One common implementation of an external optical modulator is the Mach-Zehnder interferometer [1]. Mach-Zehnder modulators are essentially photonic devices in which an input beam is split into two identical paths that eventually recombine. The optical path lengths are the same on both sides, but the phase of one beam is altered by half a wavelength by changing the index of refraction of the material the beam is propagating through. This is done by applying a voltage across the material of which a change in refractive index is desired. The result is that the two recombined beams are  $90^\circ$  out of phase with each other, creating destructive interference. There are several other implementations of beam-splitting external modulators, but they all operate on the principle of creating constructive and destructive interference through a manipulation of a material's refractive index.

Mach-Zehnder modulators have attracted significant attention due to their excellent bandwidth potential; however, there are several drawbacks that must be considered. The input light entering a Mach-Zehnder modulator must have a very narrow linewidth, which means more-expensive distributed-feedback (DFB) diodes must be used instead of standard laser diodes [2]. Additionally, the voltage-induced index change is relatively weak in most materials, necessitating a path length in the area of a few centimeters. In free-space applications, a silicon optical amplifier (SOA) must also be added to the system to increase the output signal's amplitude before transmission. The additional cost of DFB and SOA components combined with the challenge of integrating the large Mach-Zehnder modulator into compact electronic circuits, make this type of modulator disadvantageous for applications that do not demand extremely large bandwidths.

Alternatively, external modulators based on acoustic waves have also been considered [3]. These modulators effectively create a Bragg grating in a material by applying a standing acoustic wave to a crystallin structure. An optical signal is then reflected off the Bragg grating with the reflected angle related to the period of the grating. By manipulating the frequency of the acoustic wave traveling through the crystal, it is possible to change the direction of the reflected light. This system effectively controls the amplitude of the received light at the receiver by modulating the direction of a CW beam. Although this is an interesting concept, the bandwidth of this system is limited by the scanning rate of the acoustic optical modulator,

which is typically less than 100 MHz, and would simply be insufficient when FSO systems are pushing toward Gb/s communication links.

Despite the drawbacks inherent to external optical modulators, there are some applications for which they are well suited. For example, long-range FSO communication links between satellites and ground stations demand high bandwidth, high output power, and excellent beam quality. Such links have been demonstrated using Mach-Zehnder modulators, SOAs, and telescopic beam-shaping optics [4, 5]. For reasons that will be discussed later, direct-drive optical systems are much harder to collimate and therefore struggle to maintain high optical power densities over long distances. However, in short-range applications, where the bandwidth requirement is smaller and precise collimation is not necessary, direct-drive systems are superior.

### **1.1.2 Direct-drive Modulation Method**

Direct-drive modulators manipulate the amplitude of the transmitted beam as the light is created instead of altering the amplitude of a beam in steady state. This type of modulator effectively eliminates the need for separate light sources and modulator components by combining the two into a signal part. For this modulator to work, the amplitude of the transmitting light source must be current driven and fast responding. Two types of light-emitting sources meet the criteria: LEDs and laser diodes. Both devices are a type of diode that produce light by

matching the bandgap of the material that the diode is made from to the energy of a desired photon.

Laser diodes differ from LEDs in that they incorporate a resonating cavity that narrows the output spectrum of the emitted beam and increases bandwidth. The key trait that makes both devices ideal for direct-drive modulators is that the intensity of the light produced by each device is directly proportional to the current passing through the device. Additionally, both devices have a linear region of operation in which unwanted higher-order effects can be minimized. By effectively using the linear region of operation and an envelope detection method, higher-order modulation formats such as quadrature phase shift keying (QPSK) and quadrature amplitude modulation (QAM) can be implemented in direct-drive systems [6].

In FSO communication systems utilizing LEDs, direct-drive modulators are the only practical option. Unlike laser diodes, LEDs are not coherent light sources and produce light with a relatively broad spectrum. These properties prohibit LEDs from being used in systems found in the types of external modulators described in the previous section. However, high-reliability LEDs can be produced inexpensively in large quantities and can produce a wide range of wavelengths. Due to their low cost, LEDs have been incorporated into many direct-drive systems [7, 8].

Although laser diodes are typically more expensive than LEDs, they have larger bandwidths when compared to LEDs with the same power output. The two

types of laser diodes commonly used in direct-drive systems are side-emitting Fabry-Pérot (FP) laser diodes and vertical cavity surface emitting laser (VCSEL) diodes. Due to the manufacturing cost associated with fabricating FP laser diodes, they are usually more expensive than their VCSEL counterparts. However, the power output of FP laser diodes can be much greater. Using duobinary signals, FP laser transmissions of 28 Gb/s have been demonstrated [9]. VCSELs are limited to just a few milliwatts of output power, but the light that is emitted from a VCSEL's aperture is much more circular than the elliptical beam shape of an FP laser diode, and therefore, easier to collimate. VCSEL-based direct-drive FSO systems transmitting 48 Gb/s have been demonstrated without the need for equalization [10]. For short-range indoor FSO communication applications, direct-drive modulators clearly have a substantial advantage over external modulators in terms of price and complexity. Subsequently, the prototype FSO communication systems presented in this body of work will utilize direct-drive modulators.

## 1.2 Transmitter Light Source Selection

After establishing the type of optical modulator that will be used in an FSO communication system, a transmitting light source must be selected. As mentioned previously, the two main candidates for this component in direct-drive systems are LEDs and laser diodes. These two optical sources were discussed briefly in the previous section, but it is worth taking a closer look at each device. In this section,

three specific optical transmitters will be examined: LEDs, FP laser diodes, and VCSEL diodes.

### **1.2.1 LED Transmitters**

Commercially available LED light sources come in a variety of wavelengths, power outputs, and configurations. Currently, most LEDs with power outputs exceeding a few hundred milliwatts are marketed for illumination. LED luminaries have attracted the attention of several researchers as a possible dual-purpose device. The underlying argument is that the DC component of an LED luminary could provide enough light to illuminate a working area while a wireless link is simultaneously established. A high-frequency modulation signal would be added to the DC bias signal, which would be imperceptible to the human eye but detectable using a photodiode. In the commercial market today, there are two types of LED luminaries available. The first type uses a high-power blue LED that shines through a bulb coated in a yellow phosphor to broaden the luminaries output spectrum. The second type of LED luminary combines the light from a red, green, and blue (RGB) LED to create light that appears to be white. Infrared (IR) LEDs have also been used in communications systems but are not nearly as common.

For commercial lighting applications, yellow phosphor LEDs have come to dominate the market place due to the soft broad-spectrum light that they produce. Unfortunately, the yellow phosphor coating on the bulbs of these LED luminaries

dramatically reduces the bandwidth of the device. If the luminary is to be used as an FSO communications link, a bandpass optical filter must be placed on the receiver side of the link to filter out the slow-responding yellow light. Several examples demonstrating the feasibility of such a system exist [11-13]. To compensate for the limited LED luminary modulation bandwidth, advanced modulation schemes involving QAM and orthogonal frequency division multiplexing (OFDM) are usually implemented.

RGB LEDs have also experienced commercial success as luminaries, but the emitted light spectrum of these devices has been criticized as somewhat harsh and less natural feeling. However, as an FSO communication transmitter, RGB LEDs present a unique opportunity for wavelength division multiplexing (WDM). Each of the luminary's three LEDs could be used as an independent channel over which information could be transmitted. On the receiving end, three photodiodes would be required, each paired with a bandpass filter tuned to the channel's specific wavelength. This method has been shown to effectively triple the throughput LED transmitters [14, 15].

In addition to lighting fixtures, micro-light-emitting diode arrays have also been explored as a transmitting source [16]. Such arrays have been shown to have bandwidths well exceeding 100 MHz, but with output powers of less than 1 mW, these devices are entirely unsuitable for FSO applications. However, if very large arrays of micro LED could be produced, it is possible that this technology could

become useful. One distinct advantage that micro LEDs have over their larger counterparts is their tunability. With very little modification to the device structure, the center frequency of the output light can be shifted from 370 nm to 520 nm. This property again introduces an opportunity for WDM.

### **1.2.2 FP Laser Diode Transmitters**

FP laser diodes are fabricated through a process in which layers of material are grown in a sandwich configuration and then cleaved into individual devices. The resonating cavity of the laser is then formed by polishing one end of the device. The advantage of the FP laser is that the technology is very mature, which results in the availability of FP laser diodes in a variety of output powers and wavelengths. Additionally, FP laser diodes also have faster recombination times than comparable LEDs, and thus larger bandwidths. Unfortunately, the sandwich that forms the FP diode also causes the light emitted from the diode to diffract. The height of the diode's active region is very small in comparison to its width, resulting in an elliptical beam profile. Elliptical beam profiles are not necessarily problematic when a board output beam is desired, but elliptical profiles are more difficult to collimate.

Several advancements were made during the development of FP laser diodes that have improved their performance. For example, self-injection seeding of a gain-switched, multi-mode laser diode has been shown as a viable technique

for increasing bandwidth [17]. High power III-nitrate lasers have also been grown on semi-polar planes to produce FP lasers with a modulation bandwidth of 5 GHz [18]. From an application perspective, FP lasers have been used in a variety of scenarios ranging from FSO links to metro-fiber networks. In one study, a blue FP laser was used in a closed system to illuminate a glass diffuser coated in yellow phosphor; this was compared with a similar system using LEDs [19]. Although the two concepts are almost identical, the system utilizing an FP laser diode had superior brightness and bandwidth. FP lasers have also been used alongside RF signals as a method of increasing data throughput in 5G wireless networks [20]. In that demonstration, data rates of up to 10 Gb/s were achieved. FP laser diodes are certainly a viable option for direct-drive FSO communication systems; however, cost and beam quality might cause some concern.

### 1.2.3 VCSEL Diode Transmitters

VCSEL diodes differ from other laser diodes in the orientation from which they emit light. Unlike FP laser diodes, VCSELs do not need to be cleaved from a substrate before they can emit light. This is because VCSEL diodes are orientated vertically in the substrate in which they are grown and emit light perpendicularly from that substrate's surface. The unique orientation in which VCSELs are grown dramatically reduces their production costs as large numbers of devices can be grown in dense configurations and can then be tested before being separated and

packaged. Large high-power VCSEL arrays can also be manufactured very inexpensively for the same reason. The drawback of the VCSEL configuration is that the individual devices have relatively low power outputs. In general, most VCSEL diodes emit less than 2 mW. However, VCSEL diodes have been widely adopted in the telecom industry due to their high bandwidths, high reliability, and high quantum efficiencies. Recently, the bandwidth of 850 nm VCSELs has been further extended using photonic-crystal VCSEL designs [21].

In the past, VCSEL diodes were only common in guided-light communications systems; however, with the advent of inexpensive, high-power VCSEL arrays, other applications have emerged. In one such application, VCSEL arrays with power outputs well into the watt region are used to wirelessly transmit power across large distances [22]. Several researchers have also begun looking at using VCSEL arrays in FSO communications systems [23]. VCSEL arrays are particularly attractive in the latter case because they can simultaneously provide high power and high bandwidth. Unfortunately, collimating a VCSEL array with a single optical lens is impossible. The light emitted from a VCSEL array can be collected and directed using a single lens, but true collimation would require an array of micro lenses perfectly aligned with the VCSEL array. That solution is also problematic, however, because the beam waist of each of the collimated beams would be very small, resulting in a large diffraction-limited divergence. This

property makes it difficult to use VCSEL arrays in long-distance FSO communication systems but presents no problems for indoor applications.

In addition to FSO communication systems, recently, VCSEL arrays have also been explored for use in ultra-high capacity metro networks [24, 25]. VCSEL arrays present several interesting opportunities for increasing bandwidth in guided-light systems, such as constructs using several parallel channels or the introduction of WDM with individually frequency-tuned devices. These technics have been shown to yield bandwidths well exceeding of 100 Gb/s. Parallel VCSEL array driver designs have also been featured in literature with throughputs greater than 10 Gb/s per channel [26]. It is clear that VCSEL devices and VCSEL arrays are critically important technologies that will continue to dominate the telecom industry for years to come.

### **1.3 Optical Receiver Design**

In FSO communication systems, the design of the optical receiver is comprised of a photosensitive device, such as a photodiode, and a set of amplifiers. Although others exist, the two most common photodetectors are PIN photodiodes and avalanche photodiodes (APDs). PIN diodes are inexpensive, low-bias, low-noise devices that are used in almost all applications that do not require high sensitivity. APDs are similar to PIN diodes but are operated with a high bias voltage. The additional bias voltage puts the diode into an avalanche region in which the

recovered optical signal is amplified. APDs are far more sensitive than their PIN diode counterparts, but they are also much more expensive and require high-voltage circuitry. Ultra-high sensitivity, single-photon avalanche detectors (SPAD) have recently become a somewhat viable option as well, but these devices have limited bandwidth potentials [27]. SPADs are designed specifically for pulse detection and take time to recover between pulses. Advancements in the design of SPADs have brought this device closer to adoption in FSO communication systems, but further development is needed. Semitransparent solar cells have also been suggested as a way of integrating a photosensitive device into consumer electronic devices like cellphones, but these devices have extremely limited bandwidth (<1 MHz) [28].

After an optical signal is converted into electrical current, that signal must be amplified. The first amplifier that is typically used is a high-gain transimpedance amplifier (TIA). TIAs convert the photocurrent generated from the photodetector into a voltage and provide initial gain. From that point, in the case where a binary modulation scheme is used, the voltage signal is amplified by linear amplifiers or saturated by a limiting amplifier. Lastly, a clock data recovery (CDR) circuit is used to extrapolate the data and clock bits from the recovered signal. Several implementations of integrated receiver circuits can be found in the literature, including variations that include post-equalization and ambient light rejection [29].

In an effort to increase sensitivity, some researchers have also started implementing receiver designs with multiple photodetectors. Increasing the number

of detectors increases both signal strength and noise strength, but the uncorrelated noise sources only increase with the square root of the number of detectors, while the signal strength increase linearly. This results in a total signal-to-noise ratio (SNR) improvement of the square root of the number of detectors. Integrated receiver designs exploiting this phenomenon have been reported [30].

## 1.4 Dissertation Organization

In Chapter 2 of this dissertation, a hybrid FSO optical and RF wireless system is presented and characterized. In that system, a 50 Mb/s LED optical transmitter establishes a downlink while a RF WiFi router handles the uplink and provides a communication channel over which an intercell handoff mechanism is implemented. System level design considerations, hybrid system network protocol, and optical transceiver hardware design are also described.

In Chapter 3, a dual-channel, laser-based FSO system is presented utilizing both FP and VCSEL laser diodes. This chapter discusses the implementation of femtocell and attocell architectures in the context of laser-based FSO communication links. The larger femtocell is established with a 100 Mb/s, 980 nm FP laser diode, while the LOS 1.5 Gb/s attocell is established using a single collimated 850 nm VCSEL diode. Transceiver hardware design and system level implementation are described.

The design and characterization of a VCSEL array based FSO communication system is presented in Chapter 4. In this chapter, challenges in driver design strategies related to operating a high-current 500 mW VCSEL array are described and a 1.25 Gb/s optical link is demonstrated. A high-sensitivity, APD based optical receiver is also described and characterized.

Conclusions and a brief summary are presented in Chapter 5.

## CHAPTER 2. HYBRID FREE-SPACE OPTICAL AND RF COMMUNICATION NETWORKS

The number of wirelessly connected devices worldwide is currently experiencing explosive growth. Today there are more than two billion WiFi enabled smart phones and tablets, and that number is expected to increase to more than four billion by 2020. As the number of internet-connected devices continues to climb, so does the demand for data throughputs. Cisco estimates that smart devices worldwide will generate nearly 30 EB of data per month by 2020, up from less than 5 EB in 2015 [30]. To keep up with this massive increase in demand, wireless networks will have to revolutionize their infrastructure. For more than a decade, WiFi has dominated in wireless networking, and the technology has seen steady improvement during that time period; however, WiFi is intrinsically limited because it uses narrow bands centered around 2.4 GHz and 5 GHz. Recent efforts to increase WiFi data rates have led to highly efficient use of the available 2.4 GHz and 5 GHz radio frequency bands [31-33], but these efforts have not overcome fundamental limitations caused by restricted bandwidths. WiFi access points (APs) are also often shared among several users, which results in a division of the available bandwidth between each user. If the WiFi AP in question is located too close to an adjacent AP, the two signals can interfere with one another causing adjacent and co-channel congestion.

A solution to these problems can be achieved utilizing much higher carrier frequencies in the optical spectrum [34]. Optical frequencies are unregulated and do not interfere with radio signals. Additionally, optical transmissions tend to be LOS systems, which offer a physical layer of protection. Any user outside a narrow cone of light would be unable to recover the transmitted message. This LOS property impedes mobility, but also allows multiple access points to be deployed in the same operational space. Each of these access points provides an independent data link to a section of workspace through an FSO luminary. Reducing the size of the wireless cell to the area of a single light cone increases the bandwidth available to each end user by reducing the number of users accessing any given cell. In a femtocell system, the size of the cell is reduced to the point where only one or two users are accessing a wireless cell at a time [35]. This configuration results in a higher density deployment of wireless cells, but with less mobility within each cell.

In the field of FSO communication, commonly referred to as LiFi, much of the research to date has been focused on outdoor communication links [36, 37]. However, most of the problems addressed in that body of research, including long-distance attenuation, scintillation, and fading, are not present in WiFO. Although the indoor channel condition for FSO links has not been widely studied, there are several recent proposals and models detailing a joint optimization involving the simultaneous use of both RF and FSO channels [38-43]. While these works are

certainly important, they do not demonstrate a well-integrated system incorporating existing WiFi and lack a real-world demonstration of the mobility protocol.

Our approach to overcome the inherent issue of mobility in femtocell optical networks is to combine FSO and RF architectures together in a new hybrid system called WiFO. The problem that WiFO seeks to overcome is one that is very common in wireless networks: the seamless handoff from one AP to another. This problem is very difficult to solve using LOS optics, but can be easily achieved using WiFi signals. Due to the restricted size of a femtocell light cone, it is unlikely that any given user will have to share their FSO connection with many other users. As a user moves out of their light cone and into an adjacent cone, their connection can be seamlessly handed off to the next FSO transmitter in much the same way cellphone connections are handed off from one tower to the next. In this chapter, our current WiFO prototype, which provides up to 50 Mb/s of bandwidth per FSO femtocell, is presented. This system is capable of streaming data over both FSO and WiFi channels. The versatility of this hybrid architecture provides improved performance and mobility when compared to stand-alone FSO or WiFi systems.

## 2.1 Background

Recently, several efforts have been made to demonstrate the potential of FSO networks utilizing commercially available white light-emitting-diode (LED)

fixtures [44]. These fixtures are attractive because they can serve as both a visible-light communications (VLC) luminary and a communications link. However, LED luminaries are often hindered by relatively long response times, limiting their bandwidths. The two main types of LED luminaries currently under research are red/blue/green (RGB) LEDs [45] and white-phosphor LEDs [46]. RGB LEDs are often capable of higher modulation bandwidths and allow for WDM but produce a spectrum of light that is less pleasing to the eyes. White phosphor LEDs produce a warmer wide spectrum, but their modulation bandwidths are limited by the slow-reacting phosphor coating on the bulb. White phosphor LEDs are currently preferred for commercial and domestic lighting applications, and it has been demonstrated that using these luminaries as a transmitting source does not significantly degrade the quality of their output spectra [47]. Techniques such as filtering out the slower-reacting phosphor light and pre-equalizing the LED's driving circuit have been used to extend the 3dB bandwidth of white LEDs from just a few megahertz to nearly 20 MHz; however, this was demonstrated over a distance of just 10 cm [48]. The limited range of this system can be attributed to the relatively low 20% modulation depth of the transmitted optical signal.

In an effort to overcome the relatively low modulation bandwidth of LEDs, spectrally efficient modulation schemes such as QAM, OFDM, and DMT have been explored [49-51]. Although these schemes utilize available bandwidth more efficiently, they also require a significantly higher received SNR. Even a simple

four-level PAM4 scheme would require an additional 6 dB of optical output power [52]. Reducing the solid angle of the transmitting optical source can dramatically increase the power density at a receiver; however, any reduction in solid angle will result in a reduction in mobility. Well-collimated, point-to-point FSO systems have also been proposed [53], but point-to-point systems necessitate an accurate indoor positioning system, such as time difference of arrival (TDOA) [54], and a beam steering mechanism. These additional components increase complexity and reduce cost effectiveness.

In a normal office environment, the distance from the floor to the ceiling is roughly 3 m. If the average desk height is assumed to be 70 cm, any commercial FSO system must have a range of at least 2.3 m. Diffuse FSO optical transmissions of 10 Mb/s over a distance of 2.3 m have been demonstrated using white LEDs; however, the question of mobility was not addressed in that work [55].

In visible-light FSO networks utilizing LED luminaries, the power of the transmitter is directly linked to the brightness of the bulb. One solution to the brightness problem is to simply decouple the FSO network from the task of illumination by replacing the visible light LEDs with IR LEDs [56]. IR LEDs are invisible to the human eye and can therefore be driven at any brightness level without disturbing network users. Additionally, IR LEDs operating at 850 nm are inexpensive, widely available, and their wavelength corresponds closely to the peak responsivity of silicon photodiodes [57].

Regarding hybrid FSO/RF networks, work has been completed characterizing data throughputs, delay, and the effect of distance on high-performance outdoor FSO systems [58, 59]. For indoor environments, Light-Fidelity (LiFi) has been proposed as a hybrid FSO/RF system. LiFi utilizes LEDs as both transmitters and luminaries [60, 61]. One possible advantage of this model is that the power lines themselves could be used as a low speed connection between LED luminaries. This power line communication scheme could then be used to coordinate VLC transmissions between overlapping luminaries [62]. Although the integration of lighting and communications systems might initially seem like a simplification, it would require a massive shift in the manufacturing of lighting components and a complete retrofit of old lighting fixtures. In contrast, the proposed WiFO system utilizes inexpensive IR LEDs that are invisible to the human eye and do not require any integration with existing lighting fixtures [63].

From a wireless-network-design perspective, one of the critical issues that must be addressed is the handoff mechanism between APs. FSO systems can leverage some of the work compiled for RF systems; however, there are several networking challenges that are unique to LOS systems, such as the density of deployed APs. One example of this can be found in the multi-armed bandit model, which has been applied to FSO handoff strategies in an attempt to optimize the exploitation versus exploration tradeoff [64]. This model seeks to enhance the gain in a system by balancing the allocation of resources between competing users. In

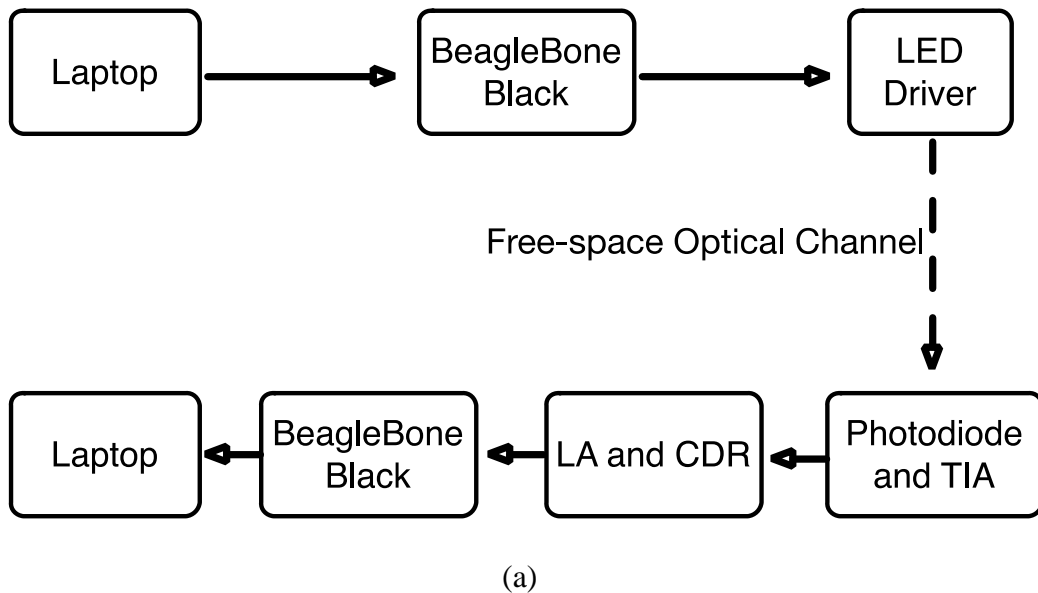
addition, the concept of fuzzy logic systems has been applied to greatly simplify complexity handoff problems [65]. Fuzzy logic systems reduce the complexity of binary decision making by transforming the problem into a list of simple rules that must be followed.

Within a single FSO AP, resource allocation must also be considered. In any FSO network, it is possible that multiple users might try to access the same optical link at the same time. If such an event occurs, it is necessary to have a system in place that can properly allocate resources to each user. To solve this problem, an automatic resource slicing or virtualization scheme has been proposed [66]. This scheme would dynamically create a number of virtual AP within each FSO cell based on the requirements of the system at any given time. In this setup, the central AP analyzes the data traffic from each of the applications supported under it and assigns resources fairly and proportionally between them. The scheduling in this system would be based on an extended token-bucket, fair-queuing algorithm, which has already been well-established for RF networks. The number of virtual slices that are required for each link can be decreased by reducing the size of the FSO AP.

## 2.2 WiFO System

In this section, the WiFO system that was constructed to demonstrate the potential of our purposed hybrid FSO and RF system is described. This system consists of an FSO transmitter and a WiFi enabled optical receiver. Both the

transmitter and receiver are connected to computers that will serve as APs through a BeagleBone microcontroller. Figure 2.1(a) shows a high-level block diagram of our system, depicting the main functional blocks of the system's components as tested. To test this system, we place the FSO transmitter and receiver on a 3 m horizontal optical rail. The receiver was also attached to a perpendicular 50 cm rail, which was used for tests involving lateral offsets. Figure 2.1(b) shows the FSO experimental setup used for testing.



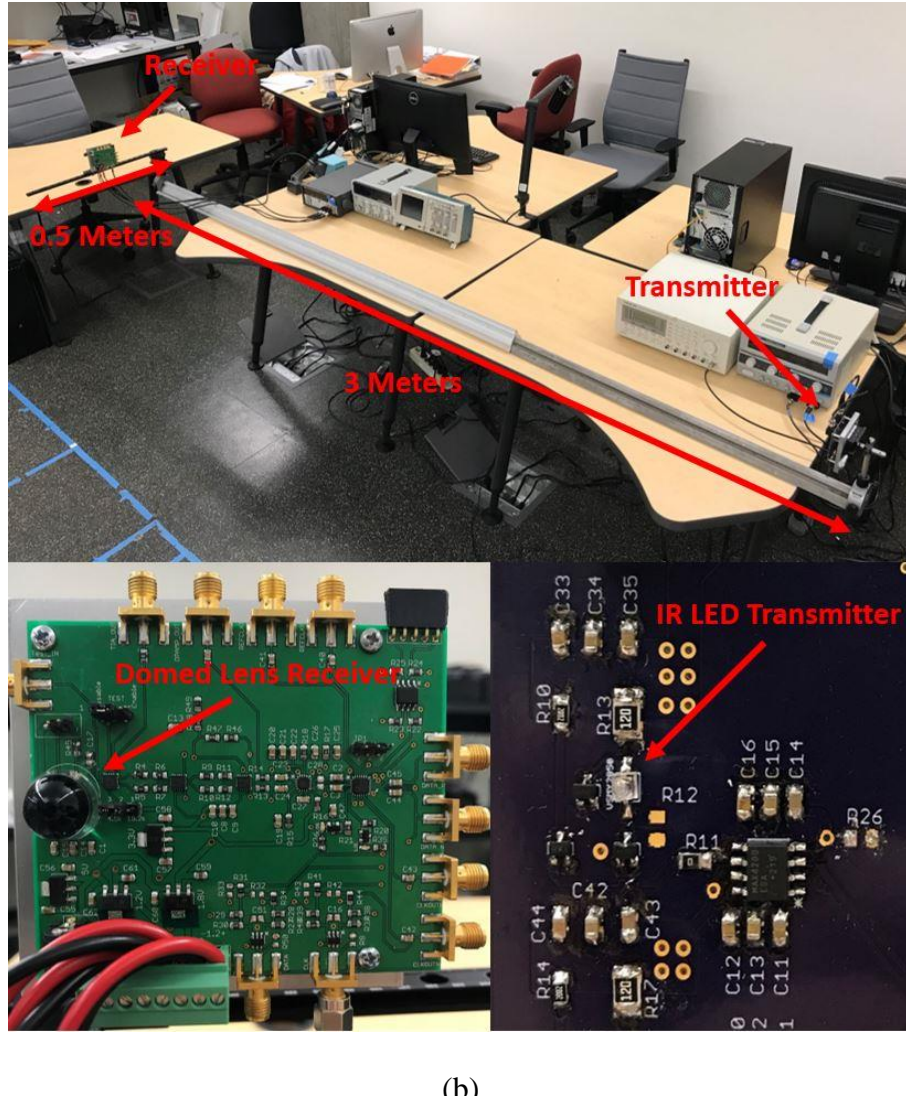


Figure 2.1: WiFO system – (a) high-level system block diagram, (b) FSO experimental setup with zoomed views of the optical transmitter and receiver

### 2.2.1 Transmitter

The transmitter component includes a BeagleBone Black microcontroller and an LED driver circuit. The BeagleBone microcontroller serves as a conduit between the AP (in this case a laptop computer) and the LED driver. On board the

BeagleBone there is a 1 GHz Texas Instrument AM335x CPU, a WiFi antenna, and 200 MHz GPIO pins. These attributes make the BeagleBone an ideal platform for sending a receiving data both through the FSO and WiFi channels. Various functions like modulation and coding on the network, link, and physical layers are handled by the BeagleBone’s PRU. After modulation and coding, the BeagleBone passes data to the LED driver in the form of binary serial bits.

The LED driver circuit is shown in Figure 2.2(a). The goal of this circuit is to convert an electrical input signal into an optical signal in a simple and cost-effective way. The main challenge in developing a robust transmitter design is overcoming the tradeoff between brightness and bandwidth. The LEDs in this design must be capable of transmitting over a distance of at least 3 m, while being modulated at frequencies in the tens of megahertz. Larger LEDs are typically brighter, but suffer from high terminal capacitance, which limit their bandwidths. In the transmitter circuit presented here, a VSMY2850 850 nm IR LED diode is modulated using a “swept-out” LED driver based on circuits presented in other works [67]. This LED driver is designed to operate the IR LED using a simple on-off keying (OOK) modulation scheme. When the LED is in the “on” state, Q3 is turned on and resistor R1 limits the current flowing through the LED, thereby controlling its maximum brightness. When the LED is in the “off” state, transistor Q2 is turned off, which in turn makes transistor Q1 high. Q1 then shorts the two terminals of the LED, reducing the optical fall time. This “sweeping out” of the free carriers remaining in

the diode improves performance by reducing the series resistance that dominates the RC delay inside the diode when switching from the “on” to “off” states. Unlike traditional LED modulation schemes, this circuit design does not modulate the LED’s brightness around a bias point. Instead the LED is driven in this two-state system in which the LED is either transmitting at its maximum possible brightness or turned off completely. Utilizing the LED’s full dynamic range maximizes the transmitter’s SNR and eliminates the need for a bias tee. Low-side driver designs that are similar to this design are also common, but often have low bandwidths due to high RC constants in the “off” state.

The improvement made in optical fall time of the transmitting LED is illustrated in Figure 2.2(b). The optical fall time without transistors Q1 and Q2 is 24 ns and is plotted in orange, while the improved 4.3 ns optical fall time, plotted as blue, is measured with transistors Q1 and Q2 in place. This 20 ns reduction in the optical fall time significantly improves the performance of the transmitter and directly translates to an improvement in the transmitter’s frequency response. Figure 2.2(c) shows the normalized frequency response of the transmitter with transistors Q1 and Q2 in place. The 3 dB bandwidth of this design is 45 MHz, which is more than sufficient for 50 Mb/s transmissions using a simple OOK modulation scheme.

The number of optical transmitters that are required to fully cover a working area is directly related to the viewing angle of the transmitting source. The IR LEDs

used in the design presented in this paper have a half viewing angle of 10 degrees. If the LEDs are placed 3 m above the ground, each LED can cover an area of 3.7 m<sup>2</sup>; however, in practice the signal will not be strong enough to serve the entire area. This coverage is largely different than that of point-to-point optical communications systems, which require aspheric lenses and well-collimated beams. Collimating the light emitted from the LED source considerably increases the power density within the beam, but also drastically restricts the angle at which the beam can be viewed.

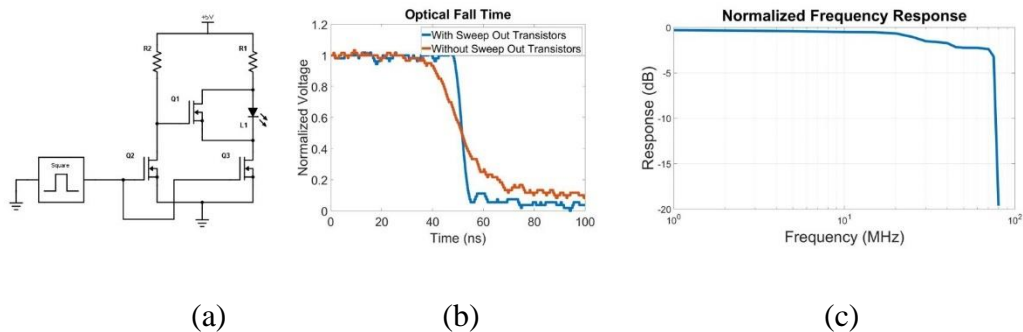


Figure 2.2: Free-space optical transmitter – (a) transmitter schematic, (b) improvement of the optical fall time with sweepout transistors included, (c) normalized frequency response

This approach is impractical for a commercial system as it greatly increases both the number of transmitters that is required within a given space and the complexity of each transmitter. Alternatively, the plastic lenses that come pre-packaged with the Vishay LEDs are available for less than a dollar each when

bought in bulk. In diffuse FSO systems, power density is usually the limiting factor and should be considered carefully. Table 2.1 lists each of the transmitter's components and their associated values.

TABLE 2.1 TRANSMITTER COMPONENTS

Schematic Symbol	Description of FSO Transmitter Components	Part Number/ Value
$Q1$	Shorts L1 when pulled high	AO7404
$Q2$	Trigger for Q1	AO7404
$Q3$	LED driver	RSU002N06
$L1$	LED source	VSMY2850
$R1$	Current limiting resistor	12 Ohms
$R2$	Pull up resistor	20k Ohms

## 2.2.2 Receiver

The receiver in this system design is responsible for collecting the transmitted optical signal and converting it back into a stream of binary bits. Due to the nature of the OOK modulation scheme used in this design, the task of recovering bits is simply a question of determining whether each bit is a one or a zero. The most straightforward means of accomplishing this task is by saturating the incoming signal and then comparing that signal to some pre-defined threshold. Figure 2.3(a) shows a high-level diagram of the receiving circuit designed around this principle. First, the incoming photons are converted into a photocurrent using a reverse-biased

PIN diode. That current is then converted into a voltage and amplified by a trans-impedance amplifier. The voltage signal is then saturated by a limiting amplifier and passed to a clock-data recovery (CDR) circuit, which outputs both the recovered bits and the clock signal that was used to generate those bits. Lastly, the recovered bits are sent to a comparator, where their amplitudes and DC levels are adjusted such that they can be directly read back into the BeagleBone Black microcontroller. The BeagleBone Black board can then directly interface with a laptop computer or transmit data back to any WiFi connected device.

In an effort to keep the cost of the receiving circuit low, inexpensive PIN diodes were chosen instead of avalanche photodiodes (APDs). APDs are often selected due to their high sensitivities, but these devices are also much more expensive. In our design, we focused on maximizing the brightness of the transmitting source, thereby reducing the need for high-sensitivity detectors. Much like the transmitting LEDs, there is a fundamental tradeoff between the size of the PIN diode's active area and its usable bandwidth. As the active area size increases, so does the diode's capacitance. This increase in capacitance then limits the bandwidth of the device by increasing its RC delay. A lens can be used to collect more light into the surface of the diode's active area, but a fundamental tradeoff between the focal length of that lens, the size of the detector, and the angle at which rays can be viewed must be considered. Additionally, there is a more general relationship between the diameter of the lens and the focal length of that lens, wherein larger lenses tend to

have longer focal lengths. These two relationships present a significant challenge for collecting light in FSO systems. Ideally, one would like to use a large lens with a particularly short focal length, which would then focus rays at large angles onto a small detector with a low RC delay, but some concessions must be made.

With these considerations in mind, a Hamamatsu S6968 PIN diode with a 14 mm plastic domed lens was selected as a receiver. This diode has a 3 dB bandwidth of 50 MHz and an effective area of  $150 \text{ mm}^2$ . Additionally, the short focal length of the domed lens mounted on its surface allows for relatively large viewing angles. Figure 2.3(b) shows a plot of the photo current generated by the diode normalized to its maximum value as a function of incident angle. From this plot, it is clear that the 3 dB half viewing angle of this diode is 30 degrees. In a real-world working environment, an FSO network user might move positions and change orientations several times. It is critical in such an environment that the optical receiver is capable of operating over a wide range of angles.

To better understand how the optical receiver in this system design will perform in an actual office setting, the receiver's sensitivity was evaluated. The sensitivity of the optical receiver is directly related to the photocurrent generated by the PIN diode. In the FSO receiver circuit, the only two components that are operating in a linear region are the photodiode and the TIA. If the TIA is generating a voltage that is greater than the minimum sensitivity of the limiting amplifier,

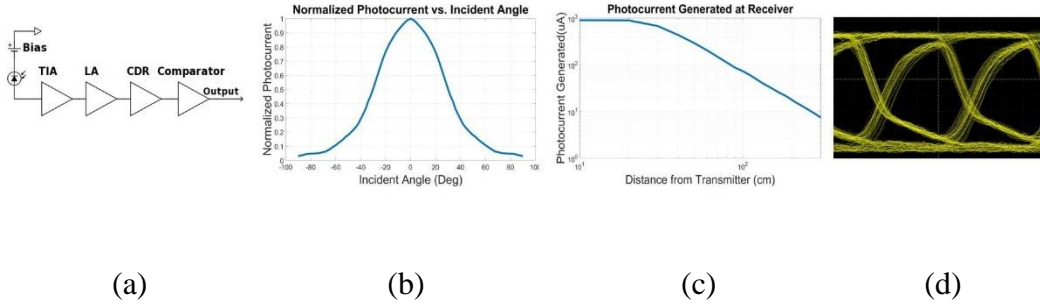


Figure 2.3: Free-space optical receiver – (a) receiver block diagram, (b) photodiode angular dependence, (c) photocurrent generated at the receiver, (d) eye diagram showing a 50 Mb/s received signal sent over a distance of 1 m before the signal is saturated by the limiting amplifier

the limiting amplifier will saturate that signal to its rail voltage. If the TIA produces a voltage below the limiting amplifier's minimum sensitivity, the output will be zero. Essentially, the limiting amplifier makes a binary decision based on the output of the TIA, and then passes either a one or zero to the CDR circuit. Once a binary decision has been made, the amplitude of the data signal moving forward is no longer a concern. For this reason, it is critical to ensure that the TIA produces a voltage that is large enough to be correctly interpreted by the limiting amplifier. Each of the receiver's components and their corresponding part numbers are listed in Table 2.2.

TABLE 2.2  
RECEIVER COMPONENTS

Schematic Symbol	Description of FSO Receiver Components	Part Number
<i>PD</i>	Photodiode	S6968-01
<i>TIA</i>	Transimpedance Amplifier	OPA857
<i>LA</i>	Limiting Amplifier	ADN2890
<i>CDR</i>	Clock-Data Recovery Circuit	ADN2915
<i>COMP</i>	Comparator	TVL3501

The Analog Devices limiting amplifier that we have chosen in this receiver design has a minimum sensitivity of  $4 \text{ mV}_{\text{p-p}}$  and the Texas Instruments TIA has a selectable trans-impedance gain of either  $4.5\text{k}$  ohms or  $18.2\text{k}$  ohms. Using these two pieces of information, it is easy to calculate that in the worst case the photodiode must generate just under  $1 \mu\text{A}$  of photocurrent to ensure that the limiting amplifier correctly interprets the data signal. Figure 2.3(c) plots the photocurrent measured from the output of the photodiode as a function of distance. The photodiode is still producing a current of roughly  $7.8 \mu\text{A}$  at  $3 \text{ m}$ , more than seven times the amplitude required for the limiting amplifier. When the photodiode is rotated such that the incident light hits the detector at an angle of  $30$  degrees, the photocurrent is reduced by about  $50\%$  to roughly  $3.9 \mu\text{A}$ . While the data signal should still be recoverable at this angle, the receiver is nearing its detection limit. Figure 2.3(d) shows an eye diagram taken at a distance of  $1 \text{ m}$  and at a data rate of  $50 \text{ Mb/s}$  before the signal is saturated by the limiting amplifier.

### 2.2.3 Network Protocol

A custom network protocol stack was created to ensure that our system hardware functioned correctly. Specifically, the physical data link, network, and transport layers were defined, and an application was created to handle the necessary data flow processes. In this section, we will provide a brief description of each layer and detail essential aspects of applications running on the ethernet-connected AP.

#### Physical Layer

On the physical layer, a simple OOK modulation scheme is used to maximize SNR. High-intensity light corresponds to a logic-high state, while low-intensity light corresponds to a logic-low state. Manchester coding is also used to ensure the regular bit transitions that are necessary for clock recovery on the receiving end. The CDR on the receiver will sample data on the rising and falling edge of the recovered clock signal. Unlike WiFi transmissions, our FSO transmitter is an LOS device, and therefore does not experience multipath fading. Reflections from objects and surfaces within the work environment do not significantly affect the received signal. Most bit errors observed in this system are caused by inter-symbol interference (ISI). This ISI is a direct result of the transmitting LED's limited frequency response.

## **Data Link Layer**

The data link layer in this stack is very straightforward. Each of the FSO link frames is broken down into a preamble and a payload. The preamble consists of 32 b and is used to distinguish one frame from another. The payload consists of 612 B and contains the data for each frame.

## **Network Layer**

The network layer in our system is different from normal network layers in that it handles the mobility protocol in addition to routing packets to their destinations. Our network layer packets consist of 12 B of packet header and 600 B of data related to the upper layers. Within the packet header, 4 B are the FSO transmitter ID, 4 B are the receiver ID, and 4 B are the packet ID. First, the transmitter ID is used to determine which transmitter will send the optical signal. Second, the receiver ID is used to determine the packet's destination if multiple receivers are paired with a single optical transmitter. Third, the packet ID is used to determine whether or not packets successfully reached their destinations. If the packets are delivered successfully, an acknowledgment is sent back to the AP. If the AP does not receive an acknowledgment for a packet, the packet ID is used to determine which packet was lost.

The AP continuously records the status of all the receivers that are active in the work area. The receiver status includes information like IP addresses, packet IDs for packets that they have received, and a transmitter ID for the transmitter that is currently associated with that receiver. When a receiver enters a WiFO network for the first time, it connects to the AP through a WiFi channel and then looks for a beacon signal. If a beacon signal is found, the receiver updates its status with the AP. If a beacon signal is not found, a timeout acknowledgment is sent to the AP and the receiver's status is again updated. On the transmitter side, the transmitter sends all the packets that it has in its queue. When the transmitter is idle, it sends out a periodic beacon signal for receivers to pick up.

## **Transport Layer**

In the proposed WiFO architecture, the FSO channel is unidirectional. Therefore, acknowledgment messages are always sent over the WiFi channel. In our system, an acknowledgment is sent for every 10 packets that are received successfully. In an effort to simplify the design of our system, the network layer, transport layer, and mobility protocol are realized in the application layer using the pre-encapsulation method. This approach will allow any future network application easy access to the WiFO system. Drivers for the FSO transmitter and receiver are being developed as a Linux kernel module.

## Access Point Application

The network protocol described in this section is implemented predominantly in an application running on a “smart” AP. The AP in this system controls the WiFi and optical transmitters and keeps track of which channels are available to end users. The application running on the ethernet-connected AP can be broken down into three main threads: data process, FSO manager, and user manager. The data process thread handles the transmission of data across both the WiFi and FSO channels. While WiFi packets are supported for both uplink and downlink, the FSO packets are only sent through the downlink. The WiFi uplink in the data process thread also relays information about the status of an end user’s connection back to the AP, which is used in the remaining two threads. The FSO manager thread controls which FSO transmitters are active at any given time. If an FSO transmitter is available to an end user, the FSO manager will activate that transmitter and direct downlink packets through the FSO channel. If the end user moves out of range of that FSO transmitter, the FSO manager will deactivate the transmitter in question. The user manager thread keeps an updated list of users on the network and tracks which uplink and downlink channels they are utilizing. When the status of an end user changes, the user manager will update its user table, which will then be referenced by both the data process and FSO manager threads. A diagram detailing the structure of the AP application, user, and FSO cone tables is shown in Figure 2.4(a) and 2.4(b). Figure 2.4(c) defines the formats of packets which keep the user

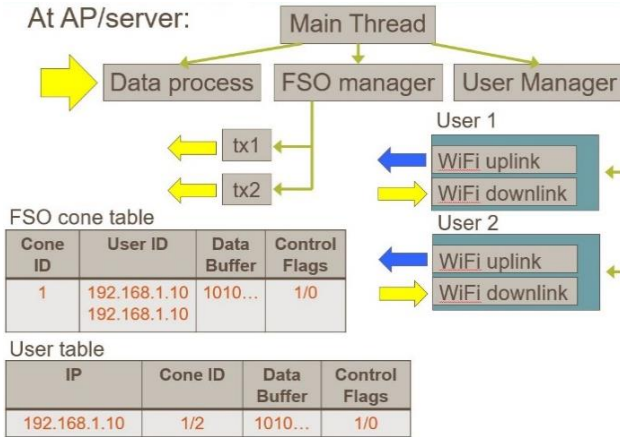
and FSO cone tables updated and ensure data transmission. The explanations of columns in the packet formats are as follows [68]:

- Cone ID: Each transmitter connected to the AP server gets a unique ID assigned by the server.
- IP Address: This stands for the destination (user) IP address of the packet.
- Packet ID: Each data packet has a unique packet ID that the AP server can track via the Ack packet if the data is received by the receiver successfully.
- Data Length: This column indicates how many bytes there are in the data payload.
- Data payload: The raw data that has not applied any modulation and coding schemes.
- Identifier: A specific number to distinguish beacon packets from the data packets.

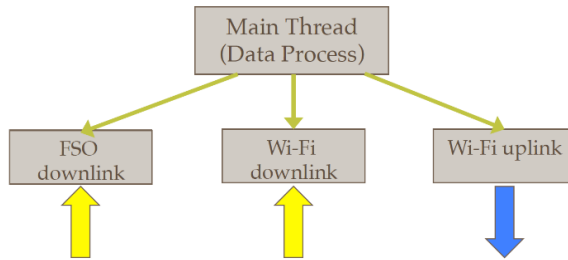
TABLE 2.3  
CONE IDS AND USERS' LOCATIONS

Cone IDs	User Location	Server Action
Current Cone ID $\geq 0$ , Previous Cone ID $< 0$	Moving into a light cone	Register the user to the table
Current Cone ID $< 0$ , Previous Cone ID $\geq 0$	Moving out of a light cone	Delete user from the table
Current Cone ID $\geq 0$ , Previous Cone ID $\geq 0$ , Current Cone ID = Previous Cone ID	Staying in a light cone	N/A
Current Cone ID $\geq 0$ , Previous Cone ID $\geq 0$ , Current Cone ID $\neq$ Previous Cone ID	Moving from one light cone to toward another	Update the table
Current Cone ID $< 0$ , Previous Cone ID $< 0$	Not moving towards or within any light cone	N/A

Data packets are encapsulated at the AP server, coded and modulated at the transmitter, and then sent to the receiver (user). Beacon packets are generated, coded and modulated at the transmitter, and broadcasted out intermittently. Ack packets are sent to the AP server from the receiver while receiving data packets/beacon packet. Upon the information in the received Ack packets, the AP server updates its user and FSO cone tables. The table below shows the corresponding user locations and server actions according to the current cone IDs and previous cone IDs from the Ack packets.



(a)



(b)

Data packet format

Cone ID (0-3 byte)	IP address (4-7 byte)	Packet ID (8-11 byte)	Data length (12-15 byte)	Payload
1	192.168.10	35	612	110101...

Beacon format

Cone ID (0-3 byte)	Identifier (4-7 byte)
1	10010100 11110110 010111101 10101100

Acknowledgement (ACK) format

Current Cone ID (0-3 byte)	Prev cone ID (4-7 byte)	IP address (8-11 byte)	Packet ID (12-15 byte)
2	1	192.168.1.10	35

(c)

Figure 2.4: AP application – (a) application diagram detailing the main threads, user, and FSO cone table formats, (b) diagram showing data process sub-threads, (c) formats of packets, which keep the user and FSO cone tables updated

## 2.3 System Evaluation

In this section we will evaluate the performance of our WiFO system in terms of transmission distance, transmission angle, throughput, bit error rate (BER), and delay. These metrics are all important factors when building a robust communications network. In each test, packets containing pseudo-random data will be transmitted across the FSO channel using a BeagleBone microcontroller as a source.

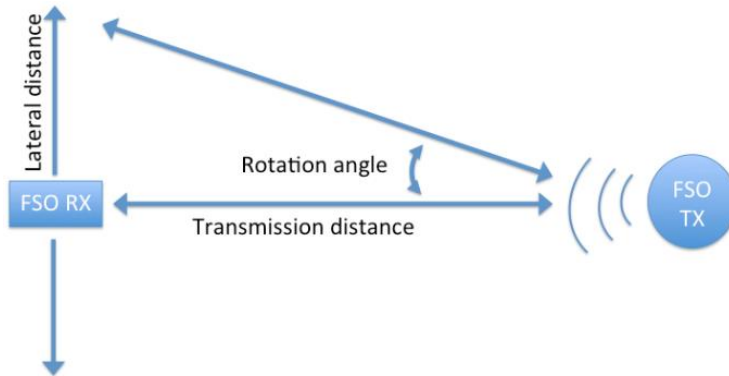


Figure 2.5: FSO channel spatial parameters

On the receiving end, the receiving module will convert the optical signal back into electrical bits and then pass the recovered data to a second BeagleBone board. The second BeagleBone will sample the recovered packets and store the data in

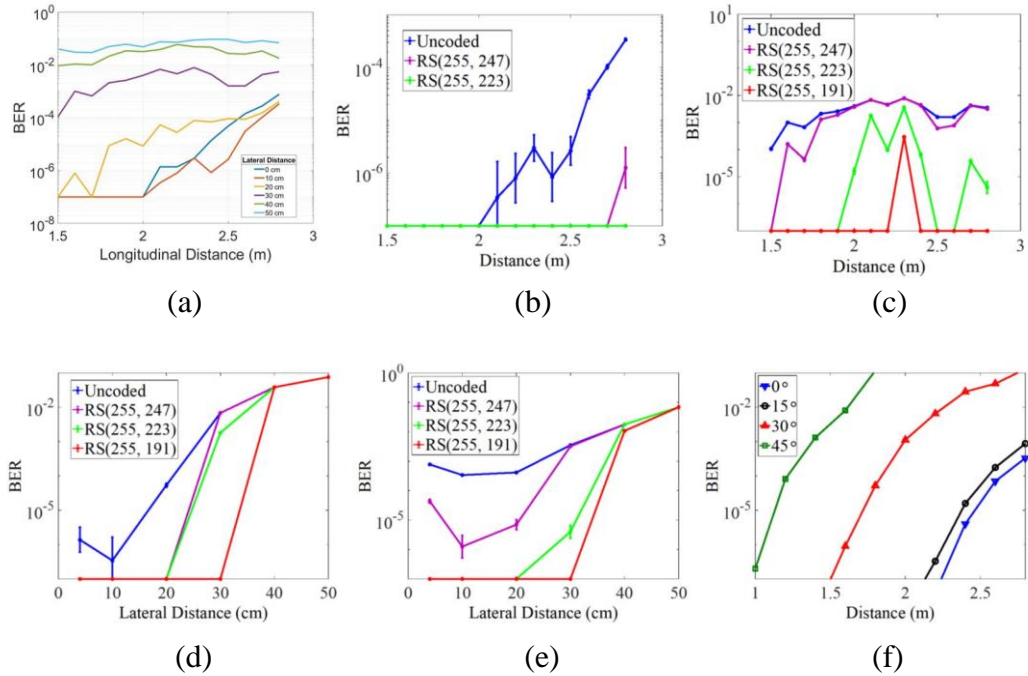


Figure 2.6: Bit error rate measurements taken at 25 Mb/s – (a) un-coded BER as a function of vertical and lateral distance, (b) Reed-Solomon coded BER with fixed .1 m lateral offset, (c) Reed-Solomon coded BER with fixed 30 cm lateral offset, (d) Reed-Solomon coded BER with fixed 2.1 m vertical offset, (e) Reed-Solomon coded BER with fixed 2.8 m vertical offset, (f) un-coded BER angular dependence

memory. In some cases, forward error correction (FEC) coding was applied to the transmitted signal in the form of Reed-Solomon codes. All measurements were taken at a data rate of 25 Mb/s unless otherwise stated. In our system evaluation we have considered several spatial parameters. These parameters are illustrated in Figure 2.5 and include vertical distance from the FSO transmitter, lateral distance between the transmitter and receiver, and the rotation angle between the transmitter and receiver. When a rotation angle is not given, it can be assumed to be  $0^\circ$ . Factors

such as FSO channel round-trip time and the transition time between the FSO and WiFi channels were also considered. Throughout this evaluation, the goal will be to achieve an un-coded BER of less than  $10^{-4}$ , which can be reduced to a BER of less than  $10^{-6}$  when simple Reed-Solomon FEC codes are applied.

### **2.3.1 Bit Error Rate without FEC**

An overview evaluation of the FSO channel BER without FEC in terms of vertical and lateral distances is presented in Figure 2.6(a). This plot shows the BER of un-coded data for vertical distances between 1.5 and 2.8 m and for lateral distances between 0 and 50 cm. Due to limitations in the BeagleBone hardware, the minimum detectable BER is  $10^{-7}$ . When the lateral distance is less than 20 cm, the BER is below the detection limit for distances less than 2 m. Interestingly, the BER for lateral distances of 0, 10, and 20 cm seem to converge as the vertical distance increases to 2.8 m. This result is most likely due to the fact that the light cone produced by the transmitting LEDs takes on a Gaussian intensity profile. As the cone diverges, points along its lateral profile do not diverge linearly. At points close to the FSO transmitter, the difference between the light intensity in adjacent lateral locations might be very large. As the Gaussian profile expands, those same points would experience a much smaller variation in intensity.

### **2.3.2 Bit Error Rate with FEC – Fixed Lateral Offset**

In all commercially available wireless communications systems, FEC is used to drastically improve the BER of transmissions. Figure 2.6(b) and Figure 2.6(c) show the BER improvements when Reed-Solomon FEC codes are applied to the data. In these figures, the vertical distance is varied while the lateral distance is fixed at 10 and 30 cm respectively. At a lateral distance of 10 cm, the weaker RS(255,247) and stronger RS(255,223) codes both reduce the BER to well within acceptable levels. In the case of the stronger RS(255,223) code, no errors were detected. When the lateral offset was increased to 30 cm, the BER increased significantly. However, the BER was again brought down to acceptable levels with the application of a RS(255,191) code.

### **2.3.3 Bit Error Rate with FEC – Fixed Vertical Offset**

In Figure 2.6(d) and Figure 2.6(e), BER measurements are recorded at fixed vertical distances and lateral distances ranging between 0 and 50 cm. The fixed vertical distances are set to 2.1 and 2.8 m respectively. In both cases, three different Reed-Solomon codes are tested. At a vertical distance of 2.1 m, even the weakest RS(255,247) code is sufficient to achieve error-free detection at a lateral distance of 20 cm. However, as the lateral distance is increased to 30 cm, only the strongest RS(255,191) provides a satisfactory BER. This trend continues when the vertical distance is increased to 2.8 m. Regardless of vertical distance and applied FEC

code, the BER in each test converges to significantly higher value when the lateral distance is increased to 40 cm. This result is expected, as the raw BER for lateral distances at 40 cm is greater than  $10^{-2}$ .

### **2.3.4 Angular Dependence**

In addition to vertical and lateral motion, rotational motion was also considered. In Figure 2.6(f), the effect of rotational motion on BER was recorded for angles ranging from 0 to 45 degrees. In each case, BER measurements were recorded as a function of vertical position with a fixed angular rotation. From Figure 2.6(f), it is clear that a rotation of 15 degrees can be reasonably tolerated, while angular rotations greater than 15 degrees significantly affect BER performance. This result is consistent with the known viewing angle of the receiving photodiode.

### **2.3.5 Bit Error Rate as a Function of Data Rate**

Next, we evaluated BER in terms of transmission speed. For this test we sent  $10^8$  pseudo random bits across the FSO channel without FEC coding and recoded the BER. This test was performed at distances of 1.6, 2.0, and 2.4 m. At each of

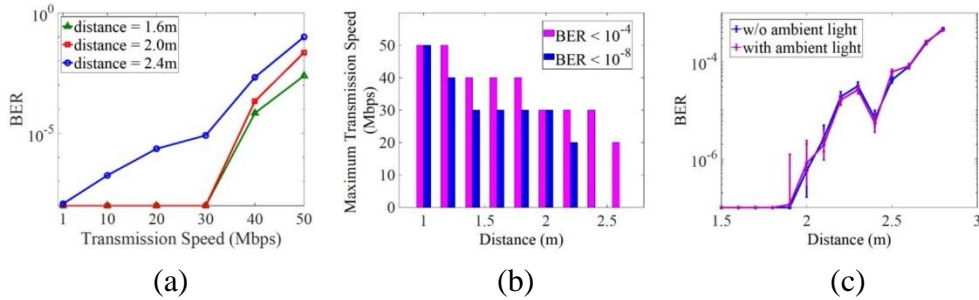


Figure 2.7: Data throughput analysis – (a) BER comparison at various data rates, (b) maximum achievable data rates given set BER requirements, (c) ambient light effect on BER

those distances, results were recorded for data rates from 1 to 50 Mb/s. The results of this test are shown in Figure 2.7(a). When the data rate is set to 30 Mb/s or less, the BER is within acceptable limits for all three distances. As the rate increases further, the BER begins to increase rapidly. Figure 2.7(b) summarizes our BER evaluation via a histogram plot containing the maxim possible transmission rates as a function of distance given a BER requirement of  $10^{-4}$  or  $10^{-8}$ . With FEC coding, a BER of  $10^{-4}$  can be converted into a BER of  $10^{-8}$  with very little overhead and is therefore a reasonable target. In its current form, our FSO system is capable of a maximum transmission rate of 50 Mb/s, although range is limited at that rate. At distances approaching 3 m, the maximum throughput for un-coded data with a BER less than  $10^{-4}$  drops to 20 Mb/s. The maximum data throughput of this system is in all cases limited by the maximum modulation speed of the transmitting LEDs. In a future version of this project, the LEDs will be replaced with much faster responding laser diodes.

### 2.3.6 Ambient Light Effect

A comparison of system performance with and without ambient light in the room was made to ensure system reliability in ambient lighting conditions. The chance of ambient light interference in our system is low because the photodiode that we selected for our receiver comes packaged with an 850 nm optical filter, but the possibility must still be ruled out. Figure 2.7(c) shows the performance of the FSO system with and without ambient light in terms of BER and vertical distance. It is clear from this plot that the ambient light in the room does not play a significant role in the performance of this system.

When considered together, the evaluations presented in this section make a compelling argument for the viability of our FSO WiFO system in an indoor environment. We have shown that this system is capable of reliably transmitting data at a maximum rate of 50 Mb/s and can transmit over distances of up to 3 m. Additionally, we have shown that the BER of this system can be significantly improved through the application of efficient Reed-Solomon FEC codes.

### 2.3.7 Evaluation of FSO and WiFi Channel Throughputs

Now that we have established the capability of the FSO channel as a standalone link, we will consider an experiment that combines both the FSO and WiFi channels together. In this experiment, we will model a scenario in which a WiFi network is artificially congested due to heavy traffic. In this scenario, two applications will be

running simultaneously. The first application will only have access to the WiFi channel. The second application will use our WiFO protocol and will have access to both the WiFi and FSO channels. The data throughput for both channels will be monitored over time as background traffic is increased and then throttled. This test will last for approximately 300 sec with the background traffic being increased after 100 sec and then decreased 200 sec later. The results of this test are shown in Figure 2.8. As expected, the throughput for the WiFi only application is significantly reduced from roughly 8 Mb/s to 3.5 Mb/s when the background traffic is increased after 100 sec. After almost 300 sec, the background traffic is throttled back to its original level and the throughput of the WiFi only application

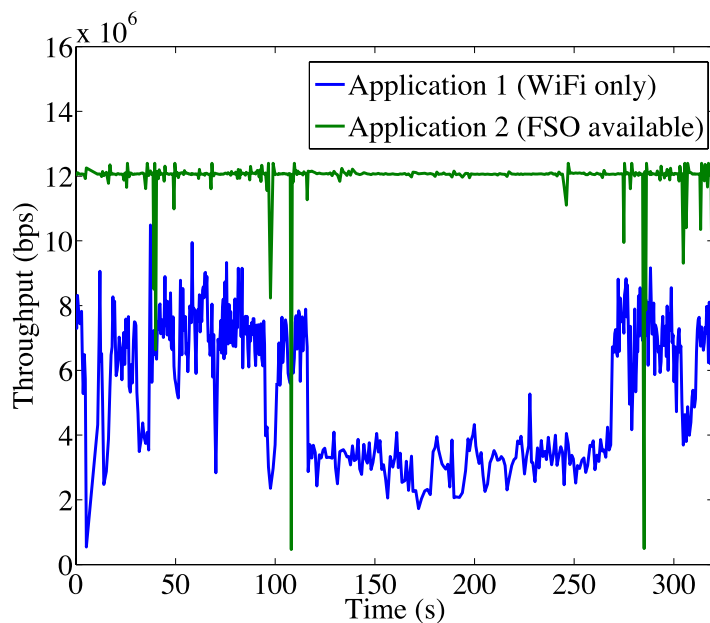


Figure 2.8: Throughput comparison between the FSO and WiFi channel

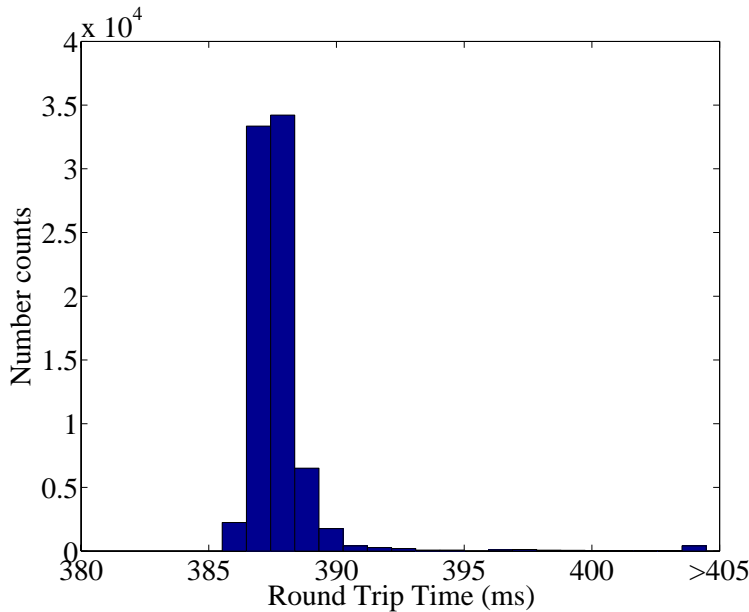


Figure 2.9: Roundtrip times in the FSO channel

increases back up to approximately 8 Mb/s. In contrast, the second application does not show any loss of throughput and maintains a 12 Mb/s link regardless of background traffic. The FSO channel in the second application provides the bandwidth and flexibility that is necessary for a consistently high-speed link. The fluctuations that are observed in the second application's throughput can be attributed to delays caused when acknowledgments from the receiver are sent back to the AP through the WiFi channel. Data was also collected on the roundtrip time for an FSO channel frame, which is the combined time it takes for a frame to be transmitted across the FSO channel and for the AP to receive and acknowledgment

of delivery. Figure 2.9 shows the roundtrip time for 80,000 frames containing 600 B each. The vast majority of frames were delivered in less than 390 ms, although some statistical outliers do exist.

### 2.3.8 Transition Time Analysis

The final aspect of our WiFO system that we will evaluate is the handoff between the FSO and WiFi channels. A smooth and immediate handoff is essential to ensuring mobility, which is a central aspect of any wireless network. When a receiver first moves into an FSO light cone, the transition time is recorded as the time between the first beacon signal and the first packet received through the FSO channel. When a receiver moves out of an FSO light cone, the transition time is recorded as the time between the receiver timeout and the first packet received through the WiFi channel. Transition times are heavily dependent on network traffic, so transition time data was collected under both heavy and light traffic conditions. The results of those measurements are shown in Table 2.4. Even under the worst-case scenario, the transition for the FSO channel to the WiFi channel, the transmission time is still less the 100 ms. That amount of time is virtually imperceptible to humans and is therefore acceptable for even latency sensitive applications. The transition time from WiFi to the FSO channel is less than 2 ms regardless of traffic conditions.

TABLE 2.4  
HANDOFF TRANSITION TIMES

	FSO to WiFi	WiFi to FSO
<b>Light Traffic</b>	49.10 ms	1.59 ms
<b>Heavy Traffic</b>	87.02 ms	1.64 ms

## 2.4 Summary

In this chapter, a novel hybrid FSO and RF wireless communication network architecture was presented. This architecture improves wireless system performance by utilizing both RF frequencies and spectrums in the optical realm. Through optimized design and integration of the optical transmitters and receivers using off-the-shelf optoelectronic devices, the FSO femtocells in this system deliver up to 50 Mb/s over a distance of 3 m with a field of view of  $\pm 15$  degrees and bit error rates between  $10^{-6}$  and  $10^{-4}$ . The bit error rate in this system was further reduced to below  $10^{-7}$  by applying Reed-Solomon FEC codes. Unlike most existing FSO systems using static optical transceivers, we achieved user mobility in this architecture through a unique WiFi-enabled protocol that allows seamless handoff between the optical and WiFi channels. We have experimentally demonstrated the potential of this WiFO architecture by comparing the throughput of our system with a standard WiFi link in a realistic use scenario. Our experimental results have

shown that our WiFO architecture is capable of expanding the capacity of existing wireless networks without sacrificing mobility.

## **CHAPTER 3. DUAL-CHANNEL FEMTOCELL AND ATTOCELL OPTICAL LINKS FOR INDOOR WIRELESS NETWORKS**

As mentioned in the previous chapter, FSO links have been suggested as an alternative to RF technologies for use in short-range wireless applications [69 - 73]. Unlike RF signals, FSO channels are LOS links that do not penetrate through walls and can be packed into high density femtocells or even ultra-high density attocells [74]. Utilizing FSO links to reduce the size of the wireless cell dramatically increases the bandwidth available to each end user by reducing the number of users on a single link. FSO links also create a physical layer of protection by necessitating that each user be placed directly under the transmitting light source [75]. Analysis has shown that the non-line-of-sight signal interference from optical transmitters in an indoor environment can be reduced to negligible levels [76 - 78].

One unresolved challenge in implementing an effective FSO system is the establishment of the uplink. It is easy to envision how optical transmitters might be integrated into the lighting fixtures of an office space or public building; however, it would be much harder to transmit optical data from a small consumer device such as a smart phone back to the AP. To resolve this issue, hybrid femtocell networks involving both FSO and RF technologies have been suggested [79, 80]. In these systems, the downlink, supporting the bulk of data transfer, would be established through an FSO channel and the uplink, comprised mainly of requests for

information, would be established via a preexisting WiFi channel. The WiFi link would also create an effective feedback mechanism, which can enable dynamic load balancing and seamless handoffs between FSO transmitters [81 - 85]. To reduce the number of optical APs that are required to service large indoor environments, and single AP with several optical transmitters pointing in angularly diverse directions, could be utilized [86, 87].

Regardless of arrangement or orientation, the key constraint when designing an effective optical communication system is the size of the optical cell. As mentioned previously, reducing the size of the cell is favorable in the sense that the number of users per cell is also reduced. However, if the optical cells are too small, a large working area would require an unreasonable number of optical cells and would reduce mobility within each cell. Additionally, there is a tradeoff between power and bandwidth. As the radius of an optical cell increases, the power that must be delivered to that cell increases at a rate of the radius squared. To overcome this problem, we propose a two-tiered FSO transmitter in which a high-speed optical attocell is placed within a medium-speed optical femtocell.

### **3.1 Background**

Current WiFi networks are inherently limited by restrictions placed on the spectrum that such networks can operate in. Spectral resources in the RF frequency range are already highly optimized, which makes improving data throughputs in

that range difficult. As a result, there has been growing interest in using optical frequencies much higher in the electromagnetic spectrum. Unlike RF signals, optical frequencies tend to be highly directional and do not effectively penetrate through barriers, such as walls. Although the idea of a standalone LiFi network is quite new, working prototypes of optical transmitters and receivers have already been demonstrated [88, 89]. These prototypes utilize inexpensive and widely available LEDs as an optical light source; however, the modulation bandwidth of LEDs operating in the hundreds of milliwatt range is typically less than 100 MHz. The modulation bandwidth of a transmitting LED can be improved by reducing the LEDs output power, but any reduction in the transmitted power will result in a reduction of the system's range and an increase in the system's BER.

One alternative method for increasing the data throughput of an optical transmitter is to use a modulation scheme with a high spectral efficiency. Typically, optical communication systems maximize SNR by using a non-return-to-zero, on-off keying (NRZ OOK) modulation scheme. However, quadrature QAM schemes utilizing OFDM have also been explored [90]. QAM modulation schemes make full use of both the amplitude and frequency signal components but require the transmitter and receiver to have flat frequency responses. As a result, QAM modulators often implement OFDM to subdivide the available bandwidth into several subcarriers with relatively flat frequency responses. Several different OFDM variants have been investigated for optical transmission including

asymmetrical clipped OFDM, direct-current-biased OFDM (DCO-OFDM), and hybrid-diversity combined OFDM [91 - 93]. While each of these methods have advantages and disadvantages, DCO-OFDM has been widely adopted for optical applications due to its direct-current component. All optical transmitters require a direct-current bias to operate properly. Although QAM OFDM modulation schemes offer much higher data throughputs, they also require higher SNRs, and therefore more demanding power requirements. That characteristic makes applying such a scheme challenging in an environment in which power density is already a primary concern.

In addition to bandwidth, mobility is also a key factor in any wireless communication system. Mobility in FSO networks is especially challenging due to the LOS nature of optical transmitters. Mobility within an optical cell can be increased by increasing the size of the cell; however, doing so significantly decreases the power density within that cell. When the size of each optical cell is small, it is imperative that the network has an effective handoff mechanism that allows users to move from one cell to the next. Hybrid WiFi and FSO networks have been investigated as one possible solution to this problem [94]. These networks use FSO transmitters as a downlink, while the uplink is handled by traditional WiFi links. When a user is in transition from one optical cell to the next, the WiFi link provides a feedback channel to the central AP. Additionally, efficient

dynamic user access in which multiple users can connect to a single AP has been demonstrated using time division multiplexing [95].

By providing an effective handoff mechanism, hybrid FSO and RF networks allow designers to arbitrarily reduce the size of the optical downlink cells. Reducing the size of the downlink cell is advantageous because it results in fewer partitions of the available network resources. Femtocells consisting of just a few users and attocells, where only a single user has access to a wireless link, have higher data throughputs and less interference than larger macrocells [96]. Optical attocells utilizing DCO-OFDM have been studied as a means of producing a robust single-user wireless link [97, 98]. Although there are many factors to consider when designing an FSO communication system, this paper will focus exclusively on the design and characterization of a dual-channel optical transmitter and receiver pair.

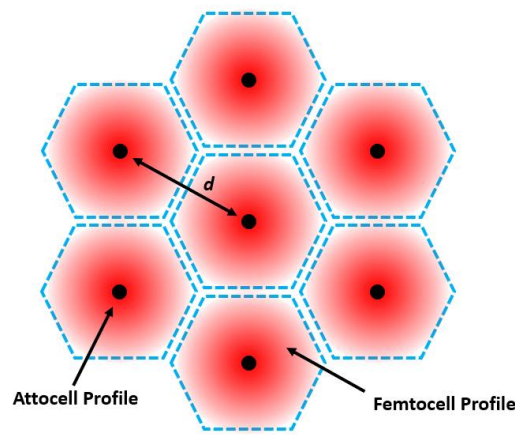
### **3.2 Dual-channel Optical Link**

When designing an FSO communications link, one of the fundamental questions that must be addressed is how large the divergent angle of the transmitting light source should be. If the divergent angle is too large, the power density at the receiver will be insufficient to recover the transmitted signal. However, if the divergent angle is too small, the area in which the receiver can detect the transmitted signal will be minuscule. Transmitted beams with narrow profiles create a substantial problem for mobility, which is a critical component of any wireless

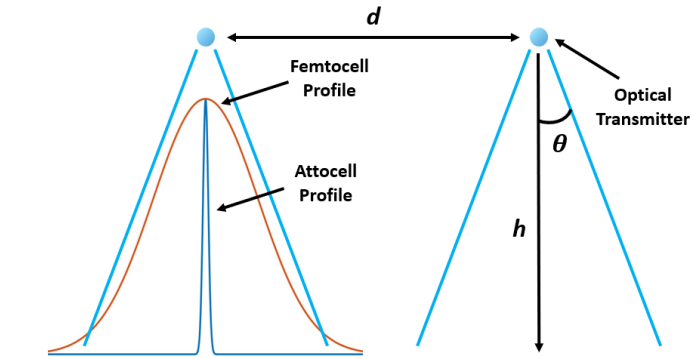
communication link. The second tradeoff that must be considered is between power and bandwidth. Increasing the power output of the FSO transmitter is clearly advantageous for improving the SNR in the link; however, doing so also tends to reduce the bandwidth of the transmitter proportionally. This reduction in bandwidth is primarily due to the necessary increase in the size of the transmitting device, which increases the capacitance of that device. When considered together, these four parameters—received power density, mobility, power output, and bandwidth—define the constraints in the design of any FSO link.

Optimization of the four parameters listed above depends heavily on the requirements of the end user. For example, if a large bandwidth is necessary, it would be easy to choose a less-powerful transmitting light source and reduce the divergent angle of the transmitter. However, doing so would severely limit mobility. Mobility could be restored by adding a beam steering mechanism that would guide the narrow beam to the user, but that type of addition would add significant cost and complexity to the system. The commercial success of any indoor FSO link will depend heavily on its ability to compete with already well-established WiFi links. If the target tracking and beam-steering components of a new FSO system push the price of the link significantly higher than that of a WiFi router, consumers will reject the new technology. Therefore, there is a large incentive for designers to select a passive optical transmitter configuration in which a cone of light is simply directed downward into a workspace. If the solid angle of

the transmitted light cone can be set to a reasonably large value, limited mobility can be achieved under each passive transmitter. Mobility in the greater FSO network can be expanded by packing multiple transmitters into a workspace as shown in Figure 3.1(a) and through the implementation of a simple handoff mechanism.



(a)



(b)

Figure 3.1: Overlapping FSO femtocell and attocell profiles – (a) top view with honeycomb AP packing, (b) side view with design constraints shown

In Figure 3.1(a), the gaussian femtocell optical profile is shown in red while the much smaller attocell profile is represented as a black dot. The distance  $d$  between the optical femtocells is determined by the power density within the femtocell and the sensitivity of the receiver. The honeycomb packing pattern shown in Figure 3.1(a) allows for optimal transmitter density. In the design of our dual channel FSO system, we will balance the needs of all users by implementing a system in which two overlapping FSO channels are available in each optical cell. The first channel will serve as a medium-speed 100 Mb/s link operating at 980 nm and will offer limited mobility to the end user, while the second channel operating at 850 nm serves as a purely LOS high-speed 1.5 Gb/s link. These two channels will be referred to as femtocells and attocells respectively. The respective wavelengths for each cell are selected in the near infrared (IR) to match the peak sensitivity of inexpensive silicon photodiodes so that they are invisible to the human eye. The separation between the two wavelengths is meant to ensure that both channels can be operated simultaneously while overlapping. On the receiving end, a narrow band optical filter will be used for the high-speed channel so that the lower-power 1.5 Gb/s signal can be distinguished from the higher-power 100 Mb/s signal. Figure 3.1(b) shows a side view profile of the dual-channel system described above.

### 3.2.1 Femtocell Design

In our FSO system, the 980 nm femtocell serves as the primary data link between the AP and the end user. The design of this optical cell will allow the users to stream data at speeds of up to 100 Mb/s without having to carefully align their computer with the transmitted beam. A 200 mW side emitting a Fabry-Pérot (FP) laser diode was chosen as the transmitting light source for this link. A simple analog driver utilizing a passive RF matching network and an enhanced-mode, pseudomorphic, high-electron-mobility transistor (E-pHEMT) was designed to meet the requirements of the FP laser diode. E-pHEMT transistors have previously been used in RF wireless transmitter applications because of their capacity for substantial drain currents and large bandwidths. An adjustable aspheric collimating lens was paired with the FP laser diode so that the divergent angle of the transmitter could be set to any desired value. A schematic of the FP laser driver design is shown below in Figure 3.2. The same general driver design is also used to drive the vertical-cavity surface-emitting laser (VCSEL) diode in the FSO attocell; however, several of the components values were modified in that design to better suite the lower power VCSEL. The component values used in the femtocell design are shown below in Table 3.1.

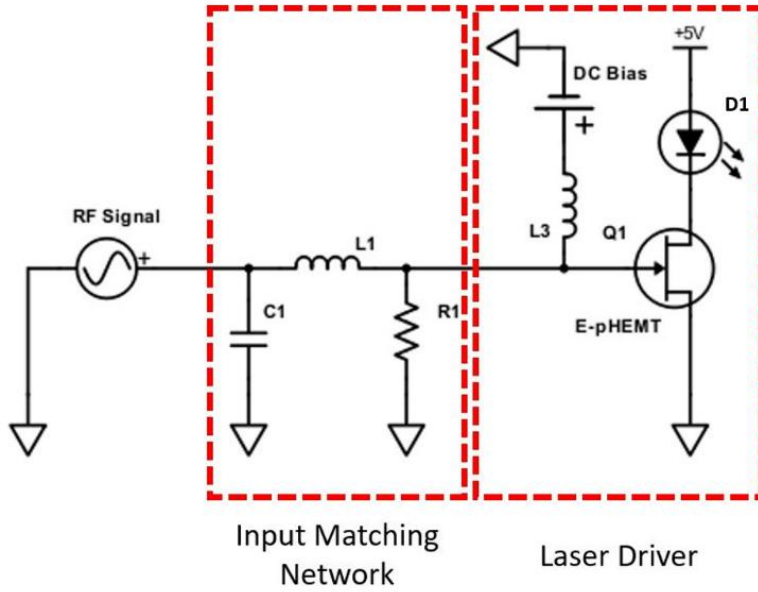


Figure 3.2: Laser driver schematic used for both the femtocell and attocell transmitters

To balance the tradeoff between power density and mobility, the divergent angle of the optical femtocell was set to  $6^\circ$ . In a standard office environment, the distance between the ceiling and the surface of a desk is approximately 3 m, therefore the diameter of the femtocell light cone at the receiver is roughly 60cm. A working spot size diameter of 60 cm is large enough that any given user can place their computer anywhere on a normal size desk and still receive a strong signal that is also small enough to ensure that the user does not have to share that connection with an adjacent user. It is important to remember that the main drive behind reducing the size of any wireless cell is to reduce the number of users accessing each cell. Ideally the number of users per cell would be just one with the density

of cells equal to the density of users. When the number of users per cell is reduced to one, the overhead associated with dividing the available bandwidth between users is eliminated and the remaining user has unfettered access to the link. In an indoor office environment, an assumption can be made wherein the ideal density of wireless links would be equal to the density of desks in that workspace.

TABLE 3.1: FEMTOCELL TRANSMITTER COMPONENTS

Schematic Symbol	Description of FSO Transmitter Components	Part Number/Value
$C1$	Matching capacitor	4pF
$L1$	Matching inductor	8.2nH
$R1$	Matching resistor	50 $\Omega$
$L2$	RF choke	7 $\mu$ H
$D1$	FP laser diode	L980P200
$HEMT$	Driving transistor	ATF11P8

### 3.2.2 Attocell Design

The 850 nm attocell in our FSO system has been designed to optimize bandwidth for applications that demand higher data throughputs. The attocell link will give users access to data rates of up to 1.5 Gb/s; however, that increase in bandwidth comes at the cost of mobility. For the attocell link, a 2 mW VCSEL diode was selected as the transmitting light source due to its high quantum efficiency and large bandwidth. VCSELs have also been widely adopted in the telecom industry because they have been shown to be highly reliable and can be

purchased at a low cost. These traits also make them very attractive for FSO communication; however, the power output of these devices is very limited. Subsequently, the divergent angle of a FSO transmitter utilizing a VCSEL diode needs to be reduced as much as possible. The resulting beam is highly collimated and LOS by nature. To gain access to the attocell link, a user would have to place their receiver directly under the attocell transmitter hotspot and would not be free to move the receiver until they no longer required the high-speed link. However, when the receiver is placed within the attocell hotspot, the user would have access to a link more than 10X faster than that of the of optical femtocell.

The design of the attocell transmitter is almost identical to that of the femtocell transmitter, but there are a few key differences. A different E-pHEMT was chosen to better match the current and bandwidth requirements of the VCSEL diode. Additionally, the component values used in the RF matching network were redesigned to provide a better match at higher frequencies. An aspheric lens was also attached to the attocell transmitter to collimate the transmitted beam. The goal of this lens is to maximize the power density at the receiver by reducing the solid angle of the transmitted beam as much as possible. Figure 3.3 shows the schematic for the attocell transmitter with the component values listed below in Table 3.2.

TABLE 3.2: ATTOCELL TRANSMITTER COMPONENTS

Schematic Symbol	Description of FSO Transmitter Components	Part Number/Value
$C1$	Matching capacitor	2.4pF
$L1$	Matching inductor	4nH
$R1$	Matching resistor	50 $\Omega$
$L2$	RF choke	7 $\mu$ H
$D1$	VCSEL diode	HFE4093-342
HEMT	Driving transistor	ATF531P8

In our experimental setup, both the femtocell and attocell transmitter PCBs were mounted to a horizontal optical rail with the attocell transmitter placed slightly under the femtocell to avoid blocking the optical path. Both transmitter boards look identical with the exception of an additional lens placed in front of the attocell transmitter. This lens is used to further focus the attocell beam on the receiver board. A picture showing both transmitter PCBs is shown below in Figure 3.3.

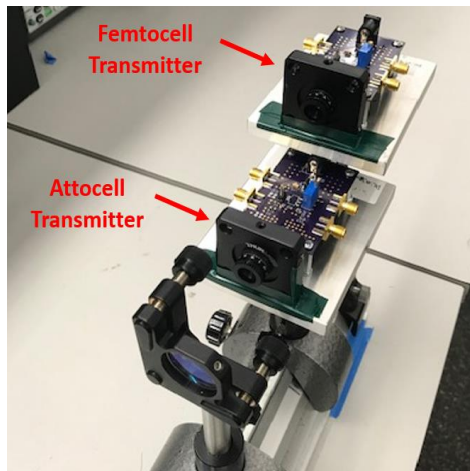


Figure 3.3: FSO transmitter PCBs showing the femtocell and attocell transmitters mounted to a 3m optical rail

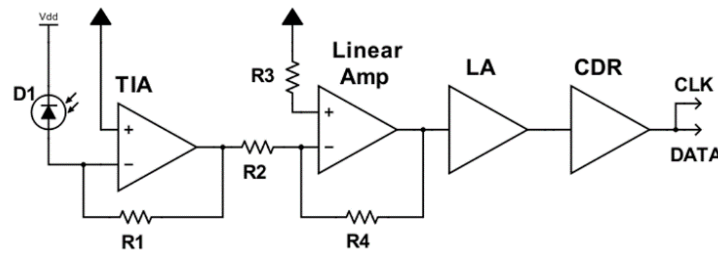
### 3.2.3 Optical Receiver Design

The FSO receiver in our system must be capable of receiving signals from both the femtocell and attocell transmitters simultaneously. To achieve this, two different photodiodes will be incorporated into the final receiver design. The size of each photodiode was chosen to satisfy the specific design constraints of each link. For the femtocell link, a large area PIN diode with an encapsulated plastic lens was selected to maximize received signal strength. The femtocell link transmitter has a relatively high-power output and limited bandwidth, which makes an inexpensive PIN diode a natural choice. However, the bandwidth and sensitivity requirements for the attocell link are much higher. Even after collimation, the power density in the attocell beam is smaller than that of the femtocell beam and the bandwidth is much higher. Therefore, the active area of the receiving photodiode diode must be smaller. To overcome these challenges, a much smaller PIN diode with a ball lens integrated into the diode's TO can package was chosen for the attocell portion of the receiver. Another issue to consider is the overlap between the femtocell and attocell links. Both receiving photodiodes are made from silicon and are therefore sensitive to both transmitted beams. This problem is solved by simply placing a 40 nm FWHM optical filter with a center wavelength of 850 nm in front of the attocell PIN. The optical filter paired with the attocell's PIN diode will reduce the 980 nm input light from the femtocell link substantially,

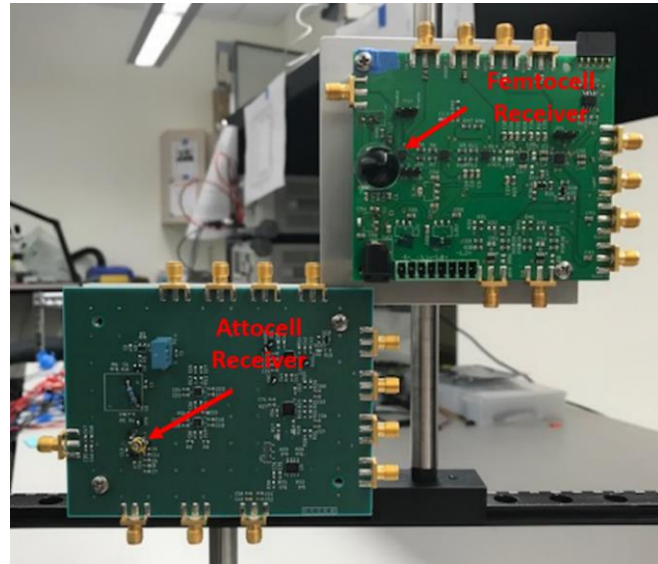
which will allow for the detection of the attocell signal. For the femtocell link, the frequency of the signal emitted from the attocell transmitter is well above the cutoff frequency of the large area PIN diode and will simply be filtered out if a user accessing the femtocell link walks directly under the attocell beam. This arrangement will allow both links to work simultaneously even when the transmitted beams of each link overlap.

The analog front end for the high-speed and low-speed photodiodes will be almost identical; however, the bandwidth of the amplifiers used in each data path will be adjusted to match the bandwidth of each photodiode. In this system, a simple NRZ OOK modulation scheme was selected to minimize complexity and maximize the SNR. As a result, the analog front end will maximize sensitivity by saturating the received signal. First, the received optical signal will be converted into a voltage through a TIA. The recovered signal will be amplified by a linear amplifier and then saturated by a limiting amplifier. The saturated signal will then be sent to a CDR circuit. In an effort to keep the prototype design of the receiver as modular as possible, the femtocell and attocell components were placed on two separate PCBs. In a later version of the project the two receiving components will be placed on a single PCB board. Figure 3.4(a) shows a schematic detailing the receiver components for both the low-speed and high-speed links, while Figure 3.4(b) shows pictures of the femtocell and attocell receivers mounted to the same secondary optical rail. This small 50 cm optical rail is mounted perpendicularly to

the larger 3m optical rail and will be used to vary the lateral position of the femtocell and attocell receivers. For continuity, locations on the larger 3 m optical rail will be referred to as vertical positions and locations on the smaller 50 cm perpendicular rail will be referred to as lateral positions. Table 3.3(a) and 3.3(b) detail the specific components used in the femtocell and attocell receivers respectively.



(a)



(b)

Figure 3.4: Dual channel FSO receiver – (a) schematic for both the femtocell and attocell receivers, (b) femtocell and attocell receivers mounted to the 50 cm lateral optical rail

TABLE 3.3 (A)  
FEMTOCELL RECEIVER COMPONENTS

Schematic Symbol	Description of FSO Receiver Components	Part Number
<i>D1</i>	Photodiode	S6968-01
<i>TIA</i>	Transimpedance Amplifier	OPA857
<i>Linear</i>	Linear Amplifier	THS4541
<i>LA</i>	Limiting Amplifier	ADN2890
<i>CDR</i>	Clock-Data Recovery Circuit	ADN2915

TABLE 3.3 (B)  
ATTOCELL RECEIVER COMPONENTS

Schematic Symbol	Description of FSO Receiver Components	Part Number
<i>D1</i>	Photodiode	S5971
<i>TIA</i>	Transimpedance Amplifier	HMC799
<i>Linear</i>	Linear Amplifier	LTC6401
<i>LA</i>	Limiting Amplifier	HMC914
<i>CDR</i>	Clock-Data Recovery Circuit	ADN2813

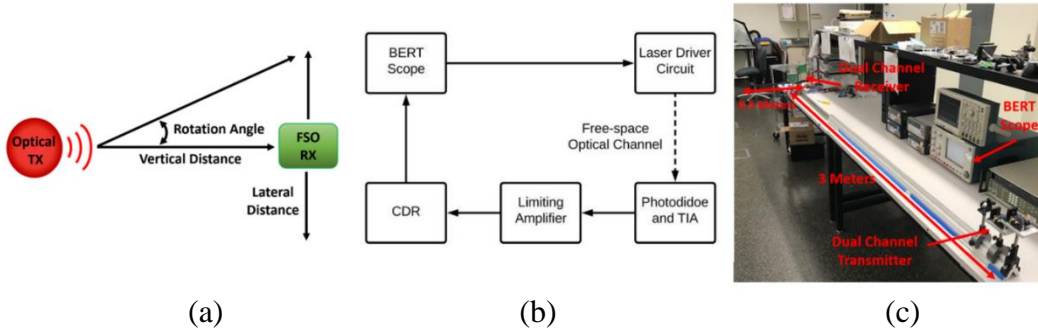


Figure 3.5: FSO dual channel test configuration – (a) diagram of relevant test parameters, (b) block diagram detailing the main components of the test setup, (c) experimental test setup with 3m vertical optical rail and 50 cm lateral optical rail

### 3.3 Dual Channel Link Evaluation

The evaluation our dual channel FSO communications system requires the evaluation of the femtocell and attocell links individually and the evaluation of both links operating simultaneously. The success of our system requires that each link perform adequately as a standalone connection and that both links also perform well simultaneously while overlapping. To demonstrate this experimentally, the femtocell and attocell links will first be tested without the presences of the other link. After those tests are complete, both links will be switched on at the same time. The results from each set of tests will then be reviewed to determine the effectiveness of our dual channel configuration. In each of these tests, the parameters of interest will include the vertical distance between the transmitter and receiver, the lateral distance between the receiver and the optical axis, and relative incident angle between the receiver and optical axis. The metric that we will use

to evaluate the performance of our system is the BER. Figure 3.5(a) shows a diagram outlining the test parameters described above.

The BER tests performed during the evaluation of this FSO communication system will all follow the same general procedure. First, a bit error rate testing (BERT) scope will generate a pseudo random bit sequence (PRBS). That sequence will serve as an input for a given transmitter under test, which will then transmit the PRBS signal across the optical channel. The receiver that corresponds to the transmitter under test will then recover the transmitted signal and send it back to the BERT scope. Lastly, the BERT scope will compare the transmitted and recovered signals and calculate a BER. A block diagram detailing the main components of this test setup is shown in Figure 3.5(b) and a photo of the test setup is shown in Figure 3.5(c). In the case of the final test in which both the femtocell and attocell are active at the same time, two different PRBS signal will be used simultaneously. The BERT scope is only capable of outputting one unique signal at a time, so an arbitrary waveform generator (AWG) will be used to produce the second signal. The eye diagrams for both signals can then be captured simultaneously on an oscilloscope.

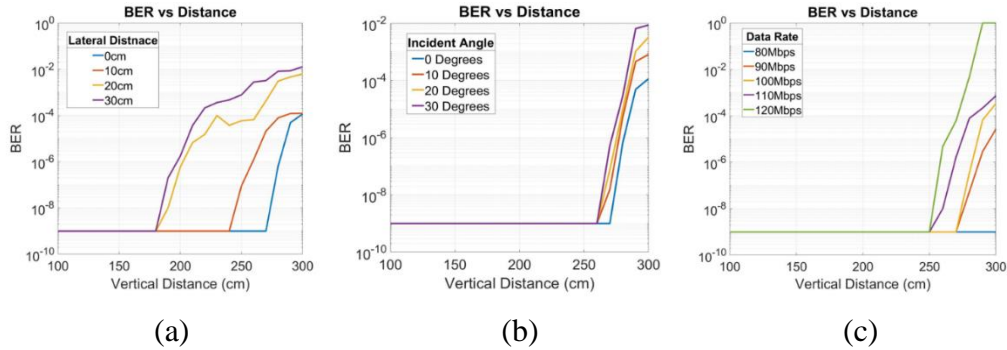


Figure 3.6: Optical femtocell evaluation – (a) BER evaluation at various vertical and lateral distances, 100 Mb/s (b) BER evaluation at various vertical distances and incident angles, 100 Mb/s (c) BER evaluation at various vertical distances and bit rates

### 3.3.1 Femtocell Performance Evaluation

In our FSO communication system, an optical femtocell will provide the main channel over which data is transferred. The goal in the design of this link is to cover as large of an area as possible while still maintaining a sufficiently low BER. In this evaluation a BER of  $10^{-4}$  will be used as a bench mark value. When the BER in a communication system drops below  $10^{-4}$ , simple forward error correction (FEC) codes can be applied to further reduce the BER by two to three orders of magnitude using well established Reed-Solomon codes. However, when the input BER rises above  $10^{-4}$  FEC codes have little or no effect on the output BER. Unless otherwise stated, the bit rate for all femtocell evaluations is set to 100 Mb/s.

Using the aspheric lens mounted to the femtocell transmitter PCB, the divergent angle of the femtocell beam was set to approximately  $6^\circ$ . At a distance of three meters, the resulting beam casts a light spot with a 60 cm diameter allowing for limited mobility within each optical cell. The relationship between vertical distance, lateral distance and BER within a single optical femtocell is plotted in Figure 3.6(a). When the femtocell receiver is placed within 10 cm of the optical axis, a BER rate of  $10^{-4}$  is achieved for all vertical distances of 300 cm or less. However, when the lateral distance is increased to 20 cm the BER exceeds  $10^{-4}$  at a vertical distance of 270 cm and at a lateral distance of 30 cm the  $10^{-4}$  cross point is 220 cm.

In addition to vertical and lateral distances, the relationship between BER and the incident angle was also evaluated. In a dynamic user environment, it is important to understand how varying the incident angle of the receiver will affect BER. The results of that evaluation are plotted in Figure 3.6(b). It is important to note that the viewing angle of the femtocell receiver is  $30^\circ$ , and for this evaluation, the femtocell receiver was placed directly on the optical axis. For vertical distances of less than 260 cm, angles up to  $30^\circ$  can be well tolerated. However, the BER increases above  $10^{-4}$  for angles in the range of  $10^\circ$  to  $30^\circ$  at distances between 260 cm and 270 cm. The close grouping of the BER traces in Figure 3.6(b) indicates that the relative change in BER is small for angular variations less than  $30^\circ$ .

The final standalone assessment that was completed for the femtocell link evaluates the effect of the link's bit rate on BER. The results of that evaluation are plotted in Figure 3.6(c). At vertical distances of less than 250 cm, error free transmission can be achieved for data rates of up to 120 Mb/s. The  $10^{-4}$  cross point for data rates of 120 Mb/s and 110 Mb/s are located at vertical distances of 240 cm and 250 cm respectively. At a vertical distance of 300 cm, the BER for a data rate of 100 Mb/s does exceed  $10^{-4}$  by a small margin. However, during previous tests, the BER was recorded as less than  $10^{-4}$  at 100 Mb/s. This discrepancy can be attributed to small variations in the testing setup between tests. For data rates below 100 Mb/s, the BER is less than  $10^{-4}$  for all distance less than 300 cm.

### 3.3.2 Attocell Performance Evaluation

The purpose of the optical attocell in our FSO communications system is to provide a high-speed link alternative to the optical femtocell for applications that demand high bandwidth connections. This link will utilize a much weaker 2 mW VCSEL diode which can be modulated at Gb/s speeds. Additionally, the wavelength of the attocell transmitter is blue shifted to 850 nm, which will allow for the addition of a bandpass optical filter on the receiving end. In this evaluation, a Thor Labs FBH850-40 bandpass optical filter with a center frequency of 850 nm and FWHM of 40 nm was used to filter out the 980 nm light transmitted from the femtocell link. Due to the reduction in transmitted power, the solid angle of the

attocell link must be drastically smaller than that of the femtocell link. At a distance of 300 cm, the diameter of the light spot cast by the attocell link is just 1 cm. This LOS link does not achieve significant mobility; however, it does provide a high bandwidth hotspot under which users can access Gb/s data rates. In the following evaluations the transmission date rate will be 1 Gb/s unless otherwise stated.

To preserve power density within the attocell link, the transmitted beam is well collimated and therefore highly directional. Unlike the femtocell link, the attocell link does not experience a rapid loss of power density over distance. It is therefore not necessary to evaluate the BER of the link as a function of vertical and lateral distance. Due to the collimated nature of the beam, the attocell link is very capable of transmitting over distances well in excess of 300 cm but cannot transmit to multiple lateral location simultaneously. As a result, the first evaluation that will be considered is a relationship between the incident angle and BER. For this evaluation, the attocell receiver is placed on the optical axis relative to the attocell transmitter at a distance of 300 cm and is then rotated. The results of that evaluation are plotted in Figure 3.7(a). Again, the bench mark for these evaluations will be  $10^{-4}$ . From the plot in Figure 3.7(a), it is clear that the attocell receiver can tolerate an angular variation of  $10^\circ$ . The limitation in angular tolerance can be attributed to the ball lens that is integrated in the TO package of the high-speed PIN diode used

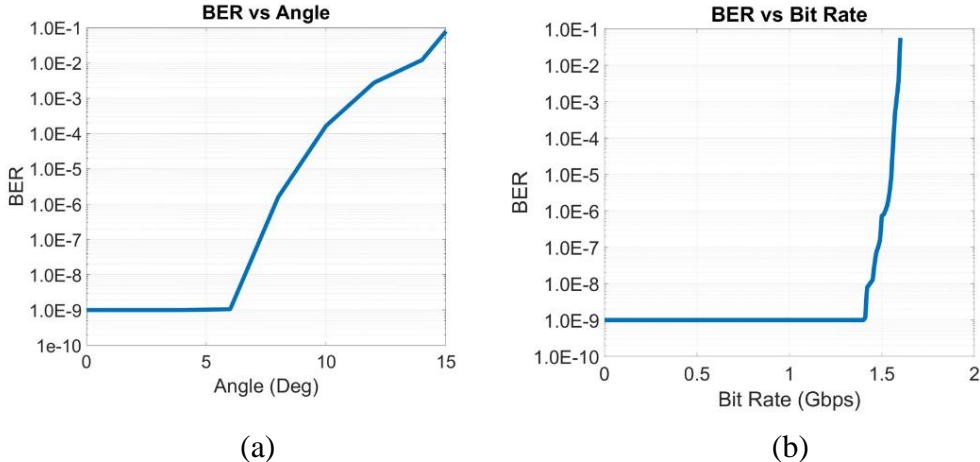


Figure 3.7: Optical attocell evaluation – (a) BER evaluation at various incident angles and at a vertical distance of 300cm, 1 Gb/s (b) BER evaluation at various bit rates and at a vertical distance of 300cm

in the attocell receiver design. This ball lens provides an important gain factor of about 4 but limits the viewing angle of the diode. Due to the LOS nature of the attocell link, a viewing angle of  $10^\circ$  is more than sufficient for this design.

The second evaluation that was completed for the attocell link demonstrates the bandwidth potential of the link. For this evaluation the attocell receiver was again placed at a distance of three meters and the relationship between the transmitted data rate and BER was recorded. The results of that evaluation are plotted in Figure 3.7(b). Error free transmission was recorded for all data rates less than 1.4 Gb/s, and a maximum rate of 1.6 Gb/s was demonstrated while still maintaining a BER of less than  $10^{-4}$ . These results show more than a 10X improvement over transmission speeds provided by the femtocell link. However,

it is important to note again that this link is strictly LOS with the attocell receiver placed directly in the path of the collimated attocell beam. In future work, mobility in the attocell link could be provided by adding a beam steering mechanism to the system. The addition of a beam steering mechanism will certainly increase cost and complexity, but such an addition could also be used to fully replace the need for a broader femtocell link.

### 3.3.3 Dual Channel System Evaluation

The final evaluation of our FSO communications system involves simultaneous recovery of both the femtocell and attocell links. To ensure that this test reflects a realistic transmission scenario, the beam profiles of each link will overlap one another as much as possible. The signal integrity of the 200 mW 980 nm femtocell link will be ensured via frequency filtering. Even if the attocell beam is incident on the femtocell receiver, the much higher frequency components of that signal will be filtered out. The signal integrity of the 2 mW 850 nm attocell link will be ensured using the FBH850-40 bandpass filter mentioned previously. This arrangement allows both links to operate in the same area without signal interference.

The test setup for this evaluation is very similar to previous evaluations with the femtocell and attocell links placed 300 cm away from their respective receivers. The BERT scope used for previous evaluations was used to generate a 1 Gb/s

attocell signal while an AWG was used to generate a 100 Mb/s femtocell signal. On the receiving end, the outputs from both receivers were connected to an oscilloscope and the eye diagrams for each signal were captured. The results of that evaluation are shown in Figure 3.8.

It is clear from Figure 3.8 that the simultaneous recovery of both the femtocell and attocell links is possible even when the profiles of both beams overlap. The strategies for mitigating intercell interference described previously were highly effective. Both eye diagrams exhibit open eye profiles and a peak to peak amplitude of approximately 1V. The evaluation of the dual channel optical communications system described in this paper was successful.

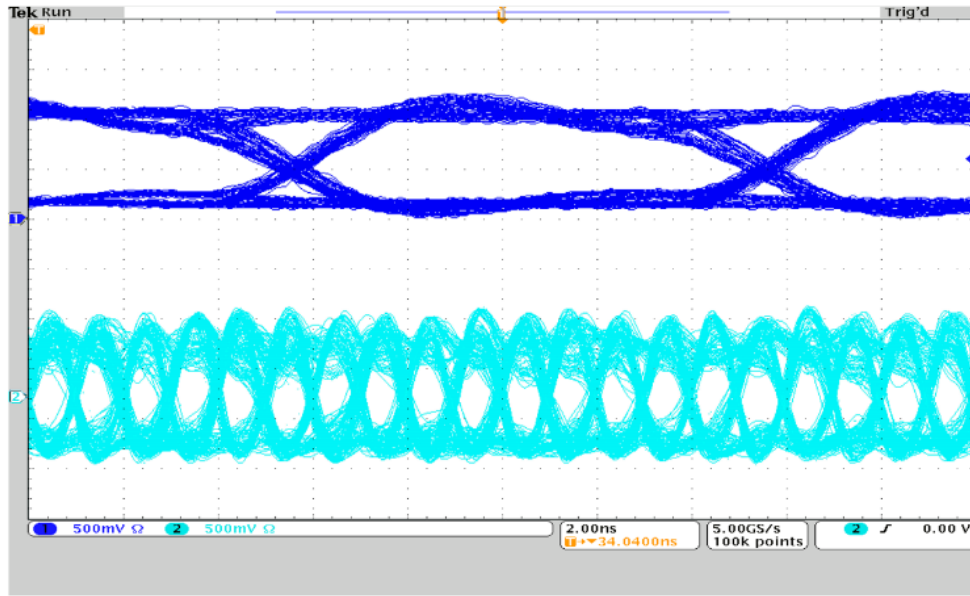


Figure 3.8: Recovered eye diagrams for the femtocell (blue) and attocell (teal) links at data rates of 100 Mb/s and 1 Gb/s respectively over a distance of 300 cm

### 3.4 Summary

In this chapter, a novel dual channel FSO communication system was presented. In this system, a dual channel femtocell and attocell architecture was described, fabricated and evaluated based on range, angular tolerance, and BER. This system consists of a 60 cm diameter optical femtocell with a 30° viewing angle based on a 200 mW 980 nm FP laser diode and a 1cm diameter optical attocell with a 10° viewing angle based on a 2 mW VCSEL diode, which is located within the lager femtocell. Both cell diameters are measured at a distance of 300 cm. The femtocell link provides a 100 Mb/s link with limited mobility, while the attocell link provides a 1.5 Gb/s LOS connection. Interference in the femtocell link was mitigated using frequency filtering, while interference in the attocell link was mitigated using optical filtering. In addition to demonstrating the potential of each link individually, we have also demonstrated the simultaneous recovery of both signals. Our experimental results have shown that this dual channel FSO system is an effective solution for providing users with both mobility enabled medium speed and LOS high speed optical links.

## **CHAPTER 4. HIGH-POWER HIGH-SPEED VCSEL ARRAY CENTRIC FSO TRANSMITTER AND LASER DIVER DESIGN**

The market success of any new wireless system will in large part be dependent on that system's ability to compete strongly with currently WiFi technology. To achieve a competitive advantage, FSO designers can leveraging preexisting technology in the telecom industry. For example, vertical-cavity surface-emitting laser (VCSEL) diodes have already been thoroughly studied, modeled, and tested as a reliable high-speed optical transmitter [99]. Adoption of these devices in the telecom industry for short-range fiberoptic networks is widespread, and advances have been made in reducing their thermal resistance [100]. Although the fabrication techniques for VCSELs have steadily improved over the years, one parameter that has remained remarkably constant is output power. Bending of the refractive layers on the top mirror of a VCSEL caused by an uneven thermal profile creates a GRIN lens effect that leads to self-focusing of the beam [101]. This self-focusing effect is referred to as thermal lensing and leads to a decrease in the single mode volume, which results in a rapid transition from single mode to multimode. Multimode VCSELs are generally disadvantageous for most applications due to their reduced efficiency and poor beam quality. The effects of thermal lensing are directly proportional to power output, so to mitigate this issue, the power outputs of individual VCSEL diodes are usually restricted to just a few milliwatts. However, the vertical-cavity configuration used in VCSEL devices is well-suited for

fabricating densely packed 2D arrays. Large 2D VCSEL arrays have been constructed on a single substrate, with each array's total output power scaling linearly with the number of array elements [102].

The development of large 2D VCSEL arrays has dramatically expanded the utility of the device. Previously, the power output of a single mode VCSEL device was limited to less than 10 mW; however, VCSEL arrays outputting more than 3 W of continuous wave (CW) power have been demonstrated [103]. These high power VCSEL arrays have become an attractive option for applications demanding intense levels optical illumination due to their high efficiency and scalability. One such application is optical wireless power transmission [104, 105]. In this application, power is transmitted from a base station to a remote location using CW laser light. The transmitted beam is then absorbed by a solar cell and converted back into electrical power. Although the efficiency of this type of system is relatively low, the technology could be very useful in challenging environments such as outer space. Another application that has attracted significant attention recently is LiDAR [106]. LiDAR systems require short, high-intensity bursts of light that are repeated as rapidly as possible. The properties that make VCSEL arrays an attractive option for this application, namely high output power and large bandwidth, also make these arrays an attractive option for FSO communication systems. In 2003, a 64-element VCSEL array outputting 120 mW of optical power was presented with a 3 dB bandwidth of 7 GHz using low thermal resistance flip-

chip bonding [107]. Later, in 2010 a 28-element array outputting 120 mW was shown to have a 3 dB bandwidth of 7.6 GHz [108, 109]. Although the 120 mW power level falls short of the power required for semi-diffuse indoor FSO systems, lower-power, short-range FSO links based on VCSEL arrays have been demonstrated [110].

In the design of indoor FSO communications networks, a fundamental tradeoff between bandwidth and power output must be considered. With the newest generation of WiFi routers approaching gigabit-per-second speeds, it is imperative that FSO links demonstrate comparable bandwidths. However, mobility is also a principle concern in any wireless network. The maximum diameter of an FSO cell is directly related to the maximum power output of a given optical transmitter and the sensitivity of the receiver. Previous work has shown that for a realistic office environment in which the distance between the ceiling and a desk is roughly 3 m, an FSO transmitter broadcasting to a femtocell with a 60 cm diameter will require an output power greater than 400 mW [111]. Based on the examples from the literature presented above, it is reasonable to believe that VCSEL array could be fabricated with a modulation bandwidth in the gigahertz range that is also capable of producing power outputs in excess of 400 mW. Deploying several densely packed optical femtocells in a working environment is beneficial in the sense that it increases the bandwidth available to each user by reducing the number of users seeking access to each cell. However, given that users might want to move freely

from one cell to the next, this configuration also creates a problem for mobility. To overcome this issue, hybrid FSO and RF networks have been proposed wherein the downlink is provided by optical transmitters while the uplink and handoff mechanisms are handled through WiFi links [112, 113]. This hybrid architecture provides users with virtually undivided access to bandwidth resources in a given optical femtocell while also providing the flexibility to move freely between cells without interruption to their wireless connection.

## 4.1 Background

Much of the work that has been done on VCSEL array based optical communication focuses on guided-light or fiberoptic systems. These systems typically use multichannel, ultra-high bandwidth transmitters with each channel being supported by a single VCSEL. The goal in these systems is not to increase the overall power output, but instead to increase the number of independent transmitters placed on a single chip. Linear VCSEL arrays supporting up to 12 channels transmitting 10 Gb/s per channel have been demonstrated [114, 115]. These linear arrays also create an opportunity for WDM due to the tunability of individual VCSEL wavelengths. Other configurations, such as circular VCSEL arrays, have been studied to support multichannel transmission in multicore fiberoptic bundles [116]. In addition to multichannel systems, devices that allow coupling of WDM transmitters into a single optical fiber are also featured

prominently in the literature. One such device is the arrayed waveguide grating (AWG). This device uses diffraction to couple several wavelengths into and out of a single mode fiber and have been shown to work effectively with up to four WDM VCSEL transmitters [117].

Each of the examples listed above utilizes a simple non-return-to-zero, on-off-keying (NRZ OOK) modulation scheme; however, several groups have also studied higher-order modulation techniques. NRZ OOK schemes are popular in optical networks because they maximize SNR and reduce complexity. In systems where the channel bandwidth is large, NRZ OOK schemes are highly advantageous because they allow designers to use non-linear saturating amplifiers that improve performance when the channel SNR is low. However, when the modulation bandwidth in a channel becomes the dominate limiting factor and SNR is not a concern, higher order modulation schemes become an attractive method for increasing data throughputs. Four-level pulse amplitude modulation (PAM4) schemes double data rate throughputs when compared to NRZ OOK, but they also reduce the SNR by two thirds. For short-range applications, an 8-channel VCSEL array transmitter was demonstrated with each channel producing a 25 Gbaud PAM4 signal, which resulted in a total aggregated data rate of 400 Gb/s [118, 119]. In addition to PAM4, schemes involving four-phase modulation have also been investigated. Quadrature phase-shift keying (QPSK) has been shown to produce symbols at a rate of 10 Gbaud when paired with an injection-locked VCSEL array

[120]. Amplitude and phase modulations have also been combined in quadrature amplitude modulation (QAM) schemes, which are often implemented with orthogonal frequency-division multiplexing (OFDM) to improve channel linearity [121]. While higher-order modulation formats might work well in fiberoptic or point-to-point free-space applications, the significant reduction in SNR makes implementing such schemes difficult in a FSO femtocell architecture.

Efforts related to producing high quality VCSEL arrays for FSO communications systems have resulted in several groups investigating coherently coupled VCSEL arrays. Coherently coupled VCSEL arrays produce in-phase photons and exhibit properties that are useful in FSO applications such as lens-free beam forming [122]. Additionally, the linewidth of a VCSEL array can be significantly reduced through coherent coupling. This reduction in the linewidth corresponds to a reduction in the divergent angle of the transmitted beam. A three-element coherently coupled VCSEL array with a divergent angle of 4 degrees and a 5x5 element array with a divergent angle of 1.61 degrees has been demonstrated [123, 124]. However, the power output of such devices was limited to just 4 mW and 10.25 mW respectively. Although the characteristics of coherently coupled VCSEL arrays appear promising, their utility will remain limited until output powers can be increased.

Much like the VCSEL arrays themselves, efforts to design appropriate VCSEL array drivers have mostly been focused on fiberoptic applications. One popular

format is a four-channel driver based on either 130 nm or 65 nm CMOS technology, providing 10 Gb/s and 20 mA per channel [125, 126]. While 20 mA might be sufficient for driving a single VCSEL, it is certainly insufficient for driving arrays of VCSELs wired in parallel. Various other improvements on the 10 Gb/s driver format have also been investigated, such as adaptive optical power control and a 12-channel radiation hardened version [127, 128]. More recently, SiGe drivers have been shown to extend data rates to 40 Gb/s per channel when paired with a single 1.3  $\mu$ m VCSEL diode [129]. While these driver designs are well suited to the single-diode VCSEL transmitters currently used in the telecom industry, they cannot provide the electrical current required to drive the high-power VCSEL arrays that will be used in the next generation FSO links.

## 4.2 VCSEL Array FSO Link Design

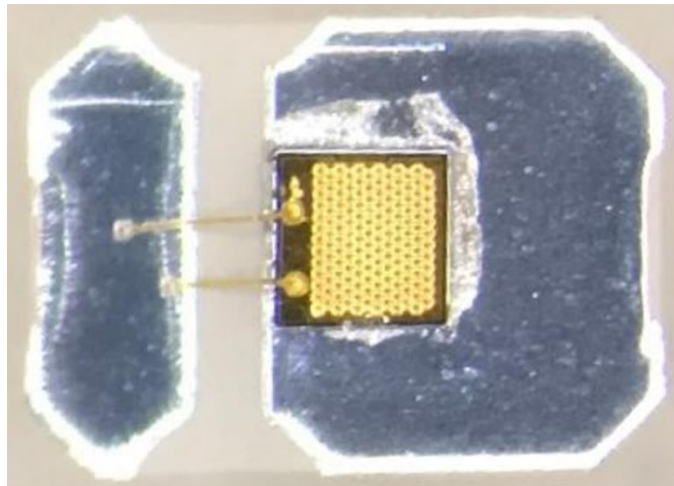
In this section, an indoor FSO communications link is described in detail. This link consists of a VCSEL array based transmitter and an optical receiver. The purpose of this link is to create an optical femtocell with an area of approximately 115 cm<sup>2</sup> that will provide a gigabit-per-second connection. The femtocell diameter was chosen to balance the demand for high-speed connections with the need for limited mobility. Mobility in this system can be further increased by packing several optical femtocells into a larger working area. Although there are several aspects of this system that require thorough consideration, such as the handoff

mechanism between FSO APs, this work will be limited to the design and evaluation of a single optical femtocell consisting of an FSO transmitter and receiver pair.

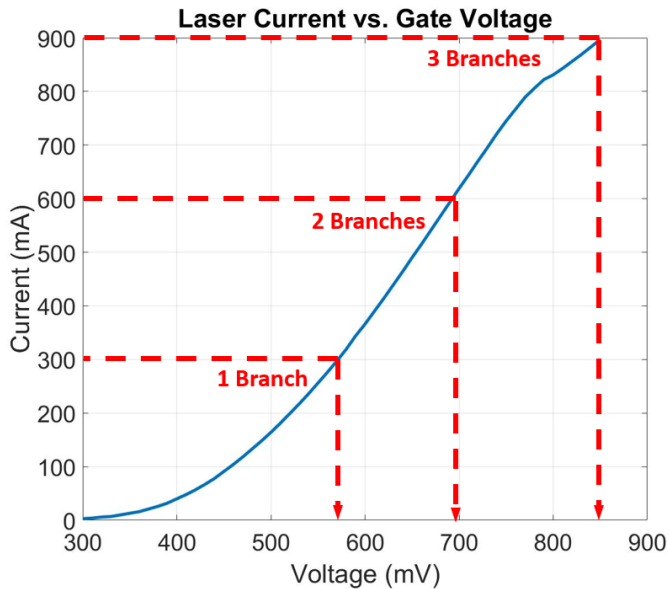
#### **4.2.1 VCSEL Array Transmitter**

In general, commercially available VCSEL arrays are wired together in parallel, which implies that the total amount of current consumed by the device is equal to the current consumed by one device multiplied by the number of devices. In the design of our VCSEL array driver, the goal is to maximize the power output of the transmitter. However, as the current consumption of the transmitter increases, it becomes increasingly difficult to design a driver that can deliver high currents at gigabit-per-second speeds. From our previous research, we have found that robust indoor optical links can be established using light sources that output a few hundred milliwatts. After considering several different devices for this project, we have decided to select a 60-element, 500 mW VCSEL array from Vixar operating at a wavelength of 850 nm. The 850 nm wavelength was chosen because it is invisible to the human eye and matches the peak responsivity of inexpensive and widely available silicon photodetectors. This device meets our requirements for bandwidth and power; however, it also necessitates a driver that can deliver up to 1 A of current. Commercially available laser drivers from companies like Texas

Instruments and Analog Devices operating at gigabit-per-second speeds are currently only offered with maximum-current ratings of a few hundred milliwatts, so a custom driver must be designed. Figure 1(a) shows a zoomed view of the Vixar VCSEL array and Figure 1(b) show the LIV curve of that device. The red dashed lines in Figure 1(b) indicate the drive current that can be sourced using one or more branches of the distributed current driver deigned for the VCSEL array. This driver design implements three parallel current paths that are then combined before passing through the VCSEL array. Each current path is capable of sourcing 300 mA, so therefore it is necessary to use all three branches when driving the array. The VCSEL array drive current is split across multiple transistors to ensure that the capacitance of each driving transistor is not excessively large.



(a)



(b)

Figure 4.1: 850 nm VCSEL array light source – (a) image of the 60-element VCSEL array device, (b) VCSEL IV curve showing various regions of operation

Much like the VCSEL array, the design of the laser driver needs to strike a balance between the size of the transistors used in the driver and the bandwidth of those devices. To the best of our knowledge, there are no commercially available transistors that are capable of sourcing 1 A of current with a bandwidth range of direct current to 1 GHz. As a result, we will need to distribute the current load between several transistors in parallel. This distributed design will allow us to scale up the total current drawn through the VCSEL array without sacrificing bandwidth. For the device selection, we will again leverage technology designed for the

telecom industry. The challenges inherent in the design of telecom transmitters are very similar to the challenges that we face now.

Enhanced-mode, pseudomorphic, high-electron-mobility transistors (E-pHEMT) have been widely adopted for wireless driver applications due to their high-linearity, high-drain currents, and large bandwidths. However, E-pHEMTs also typically have large gate capacitances. Driving a large capacitance at high speeds becomes problematic because it is more difficult to match the impedance of a large capacitor to the  $50 \Omega$  signal source at high frequencies. This is because the capacitor will present a small impedance in parallel with any matching elements that are used, which will result in a total impedance of less than  $50 \Omega$ . In RF designs, this problem is solved using a narrow-band resonate-matching network that can be tuned to a desired transmission frequency. However, this technique eliminates the possibility of using lower frequency components, and is therefore unsuitable for OOK modulation schemes, which are typically used in optical communication systems. The goal for this project was to achieve a wideband match that extends from direct current to the highest frequency possible. To accomplish this goal, we restricted ourselves to an E-pHEMT with a smaller gate capacitance and placed a  $50 \Omega$  resistor between the transistor gate and ground. This arrangement resulted in an excellent match at low frequencies. As the input frequency increased, the output signal strength gradually deteriorated as the load impedance dropped below  $50 \Omega$ . After a transistor with an appropriate bandwidth was selected, the current

requirement for the VCSEL array driver was met by placing three of the selected transistors in parallel. Table 1 summarizes the capacitance and maximum drain currents for three of the E-pHEMTs devices that were considered.

TABLE 4.1: E-pHEMT DEVICE SUMMARY

Device	Capacitance @ 1 GHz	Maximum Drain Current
<i>ATF-511P8</i>	15.02 pF	1000 mA
<i>ATF-531P8</i>	3.82 pF	300 mA
<i>ATF-55143</i>	0.85 pF	100 mA

To evaluate the bandwidth of each of these devices listed above, the S11 parameters for each transistor were simulated using Advanced Design System (ADS) simulation software. The results for those simulations are shown below in Figure 2. For the purpose of evaluating each transistor, the useable device bandwidth was defined as the -10 dB crossing point, at which point 10% of the total power is reflected. Above the -10 dB crossing point signal strength declines rapidly. The goal set forth in this paper is to achieve a gigabit-per-second free-space link, which requires a modulation bandwidth of 500 MHz using an OOK modulation scheme. It is clear from Figure 2 that the most appropriate transistor is an ATF-

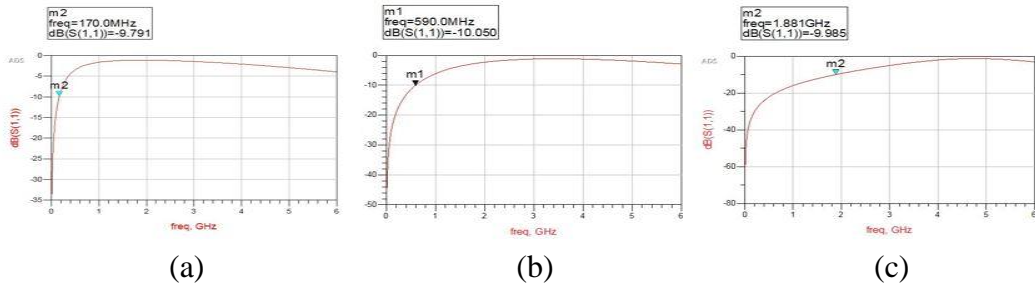
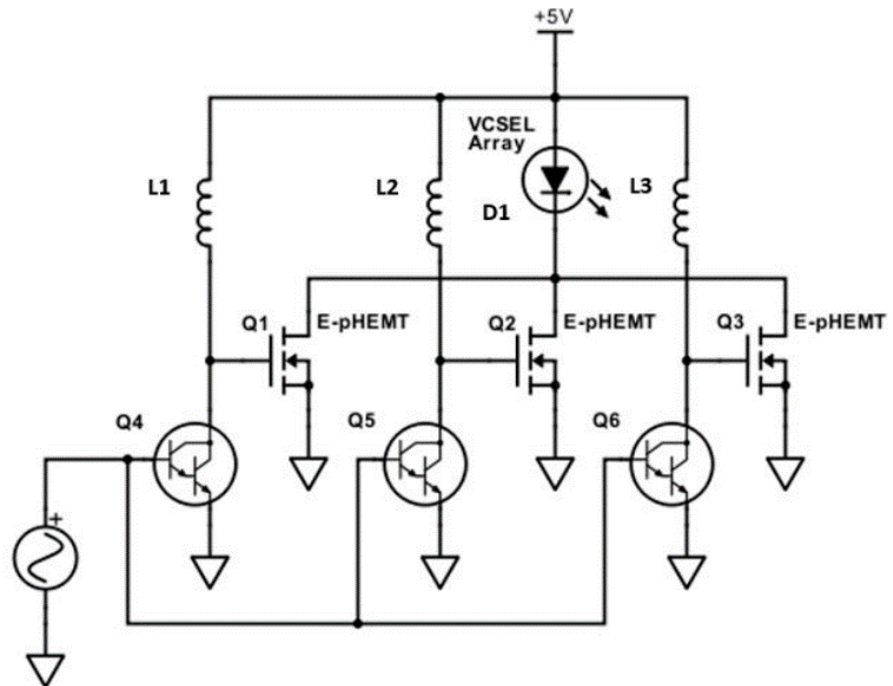


Figure 4.2: S11 simulations of E-pHEMT devices – (a) ATF-511P8, (b) ATF531P8, (c) ATF-55143

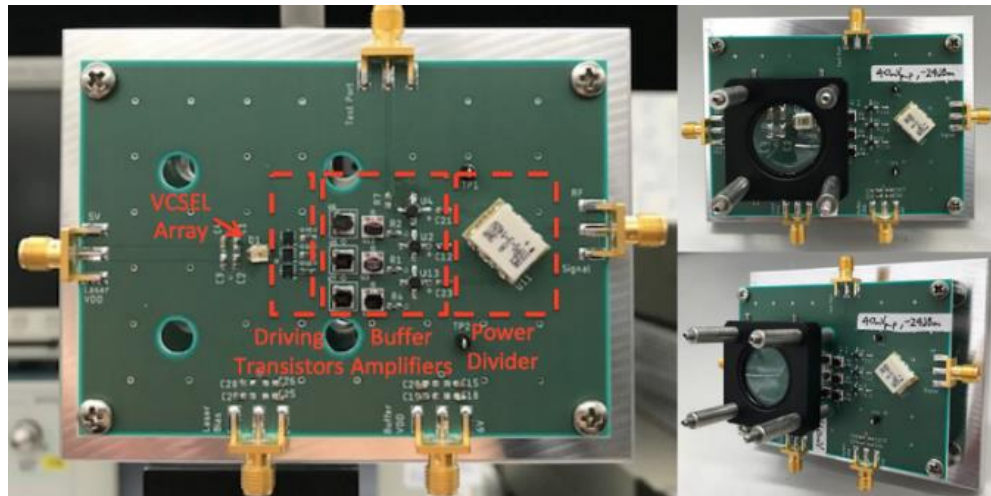
531P8 with a modulation bandwidth of 590 MHz and a maximum drain current of 300 mA. A VCSEL array driver employing three ATF-531P8 transistors in parallel could achieve a current swing of 900 mA, thereby maximizing the modulation depth of the 500 mW Vixar array.

Another aspect related to the transmitter design that needs to be considered is the combined gate capacitance between the three driving transistors. If each of the three ATF-531P8 transistors is not buffered, their combined gate capacitance will improve linearly, creating a severe bandwidth limitation. To avoid this problem, each of the driving transistors was paired with a smaller buffer amplifier. The primary requirement for the buffer in this design is that it the amplifier must be exactly  $50\ \Omega$ . Additionally, the bandwidth of the buffer amplifier must match or exceed that of the driving transistor. The buffers that we selected for this design are simple Darlington pair amplifiers.

In summary, our VCSEL array driver design consists of three current branches with each current branch driven by a 300 mA ATF-531P8 E-pHEMT transistor. At the input of each E-pHEMT transistor, a passive RF matching network is designed to ensure that there is a  $50 \Omega$  impedance match from direct current to 1 GHz. Each ATF-531P8 transistor is buffered by a Darlington pair amplifier to reduce the overall capacitance seen at the input of the driver. A  $50 \Omega$  three-way power divider is also placed at the driver's input to eliminate any impedance mismatch caused by the splitting of the input signal between the three current branches. A schematic showing the design described above is shown in Figure 3(a). The PCB designed for the FSO transmitter also has four large drill holes so that an aspheric collimating lens from Thor Labs can easily be fitted to the VCSEL array. Figure 3(b) shows the fabricated transmitter PBCs with and without a collimating lens attached. Table 3 lists the components used in the VCSEL array transmitter.



(a)



(b)

Figure 4.3: VCSEL array transmitter – (a) schematic of distributed current VCSEL array driver, (b) fabricated transmitter PCB with and without a collimation lens mounted

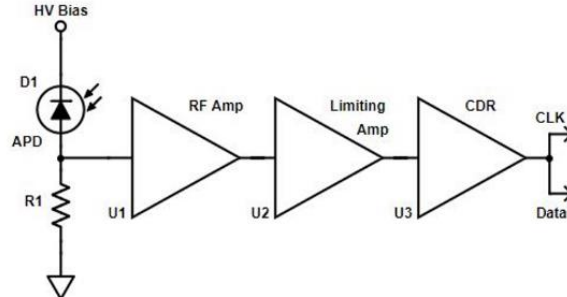
TABLE 4.2: VCSEL ARRAY TRANSMITTER COMPONENTS

Schematic Symbol	Description of FSO Transmitter Components	Part Number
$D1$	VCSEL Array	850M-0000-KP03
$L1, L2, L3$	RF Choke	TCCH-80
$Q1, Q2, Q3$	E-pHEMT	ATF-531P8
$Q4, Q5, Q6$	Darlington Pair	MAR-6SM
$PD$	Power Divider	SYPS-3-142W

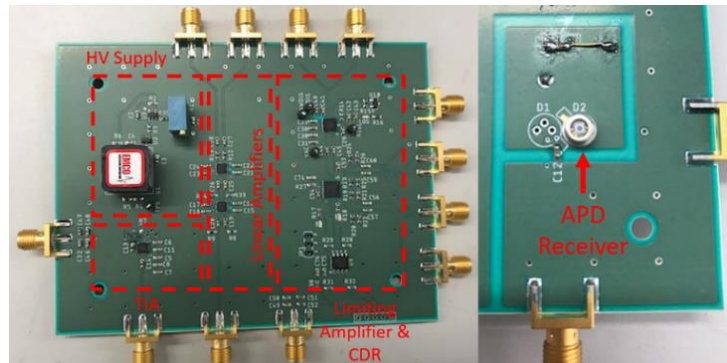
### 4.2.2 FSO Link Receiver

The effective design of a high sensitivity optical receiver is critical to the success of any FSO network. Optical power densities on the receiving end of a free-space channel are always a concern when designing optical links, so we have chosen to use avalanche photodiodes (APDs) in our design. APDs are advantageous in applications that require high-sensitivity detectors due to their large intrinsic gain. The analog front end of our receiver will consist of a standard data path, including a transimpedance amplifier (TIA), linear operational amplifiers (op-amps), a saturating limiting amplifier, and a clock-data recovery circuit (CDR). When the initial design for the receiver was created, the exact requirements for amplification on the receiving end were unknown, so the receiver PCB design was left as modular as possible. The receiver PCB was split into three main blocks that are each terminated by a SMA connector. These three blocks can be connected in any order using SMA cables. Block 1 will consist of a high-voltage DC-DC converter that provides a bias voltage to the APD, the APD itself, and a TIA to

convert the photocurrent into a voltage. Block 2 consists of two linear op-amps with a total combined gain of 100X. The final block combines the limiting amplifier and the CDR. When connected in series, these functional blocks operate as a highly sensitive optical receiver. However, if the gain in the system is too large, Block 2 can be bypassed to reduce gain. Figure 4(a) shows a schematic of the FSO receiver described above and the fabricated PCB is shown in Figure 4(b). Table 2 lists the components that were selected for each function.



(a)



(b)

Figure 4.4: High-sensitivity optical receiver – (a) block diagram detailing optical receiver data path, (b) optical receiver PCB shown with functional block on the front of the board and an APD mounted to the back of the board

TABLE 4.3  
OPTICAL RECEIVER COMPONENTS

Schematic Symbol	Description of FSO Receiver Components	Part Number
<i>D1</i>	Photodiode	S12023-10
<i>U1</i>	Transimpedance Amplifier	HMC799
<i>U2</i>	Linear Amplifier	LTC6401
<i>U3</i>	Limiting Amplifier	HMC914
<i>CDR</i>	Clock-Data Recovery Circuit	ADN2813

### 4.3 FSO Link Evaluation

In this section, the FSO transmitter and receiver pair that are described in this paper are evaluated in terms of bandwidth, range, and angular tolerance. In each evaluation, a bit error rate testing (BERT) scope will be used to generate data in the form of a pseudo-random bit sequence (PRBS). The PRBS signal is then fed as an input to the VCSEL array FSO transmitter and converted into an optical signal that is transmitted across the FSO channel. On the other end of the FSO channel, the optical signal is recovered by our receiver and converted back into an electrical signal, which is then passed back to the BERT scope. The BERT scope compares the recovered signal with the original signal and calculates a bit error rate (BER) value. A block diagram detailing this process is shown in Figure 5(a).

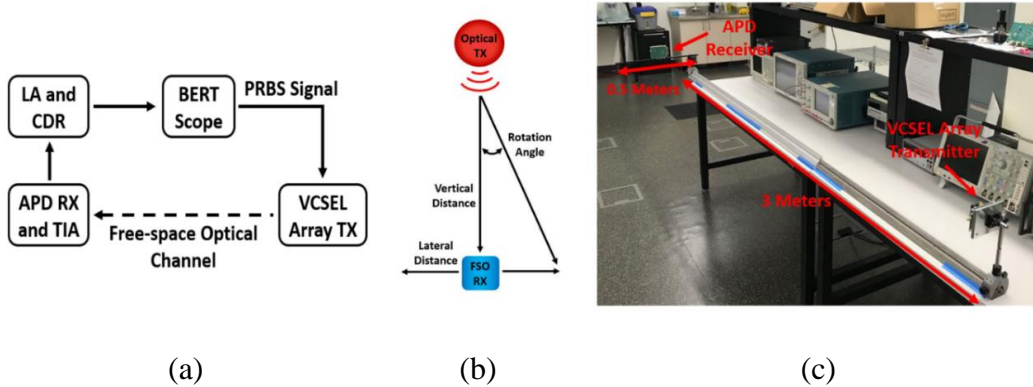


Figure 4.5: FSO channel test configuration – (a) block diagram detailing the components used in the test configuration, (b) diagram showing the FSO test parameters, (c) a photo of the experimental setup showing the 50 cm optical rail mounted orthogonally to the 3 m optical rail

The VCSEL array transmitter in this system is mounted to a horizontally positioned optical rail. The optical receiver is mounted to a second 50 cm optical rail that is positioned perpendicular to the first rail at a distance of 3 m from the transmitter. For the sake of continuity, positions on the larger rail will be referred to as vertical positions and positions on the smaller rail will be referred to as lateral positions, as illustrated in Figure 5(b). Additionally, the receiver is also mounted to a rotational stage, which can be used to change the incident angle of the transmitted beam with respect to the receiver PCB. In this experimental setup, three degrees of freedom are used to realistically model how a user might move within a FSO communications femtocell. A photo showing the implementation of this experimental setup is shown in Figure 5(c). In the subsequent system evaluations, the vertical distance will be fixed to 3 m to roughly mimic the

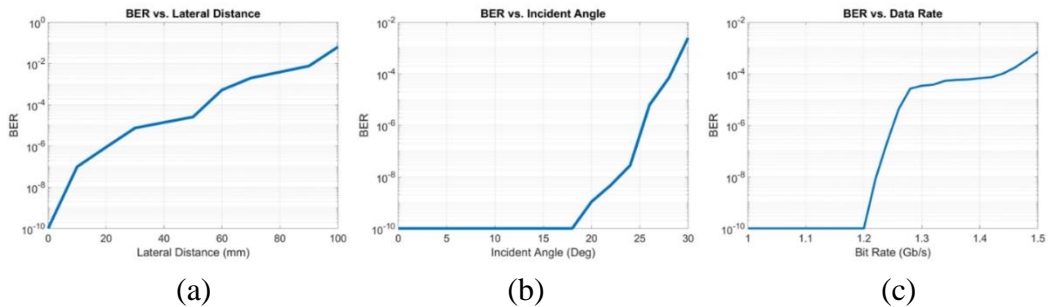


Figure 4.6: FSO system BER measurements collected at a distance of 3 m – (a) BER as a function of lateral motion, (b) BER as a function incident angle with respect to the optical receiver, (c) BER as a function of data throughput

distance between the ceiling and floor in a standard office environment. Unless otherwise stated, binary OOK symbols are used as the default modulation format.

Although the BER requirements of various data systems can vary widely, a value of  $10^{-4}$  is used as a benchmark in this paper. When the BER rate in a communications system drops below  $10^{-4}$ , common forward error correction (FEC) codes, such as Reed-Solomon codes, can be applied to the data to dramatically lower the BER. For example, the Reed-Solomon code RS(255, 247) can reduce the BER in a system from  $10^{-4}$  to  $10^{-8}$  with an efficiency of 96.8%. However, if the BER in a system is greater than  $10^{-3}$ , FEC codes will have little or no effect on the system's performance.

### 4.3.1 Lateral Motion Tolerance

Due to the highly directional nature of FSO transmissions, it is necessary to align the optical receiver such that it is located within a cone of light projected from the transmitter. As the solid angle of the transmitted light cone increases, the system becomes more tolerant to lateral movement within the FSO cell. However, if the solid angle of the projected light cone becomes too large, the optical power density within the light cone will drop below the detection threshold and the wireless connection will be lost. This tradeoff between mobility and signal strength is fundamental to all FSO systems and must be balanced to suit the needs of potential users. In our FSO system, the optical transmitter that we have designed maximizes both power output and bandwidth using a 60-element array of high-speed VCSEL diodes. This configuration allows for gigabit-per-second data rates while still providing limited mobility.

Using the experimental setup described above, BER measurements were collected at various lateral positions 3 m away from our FSO transmitter and plotted in Figure 6(a). The data rate for those measurements was set to 1.25 Gb/s. Applying our BER benchmark of  $10^{-4}$ , we defined the useful light spot diameter to be approximately 11 cm. Although user mobility is still highly limited in this configuration, the optical spot size is still quite large when compared to FSO communications systems with similar throughputs.

Optical transmission at 1.25 Gb/s has been demonstrated using a three-channel red/green/blue WDM LED luminary; however, the transmission distance was limited to just 10 cm and was strictly point-to-point LOS with no tolerance for lateral motion [130]. Similarly, high-speed laser transmitters based on single VCSEL devices have been reported [131]. However, with power outputs of <2 mW, these transmitters require precise collimation and a receiver-side focusing lens to achieve sufficiently high optical power densities. Point-to-point LOS systems are difficult to implement in realistic working environments and are therefore disadvantageous for indoor FSO communications systems. The VCSEL array transmitter presented in this paper does not require careful alignment with an optical receiver and therefore provides a level of flexibility that is necessary for commercial systems. Mobility in future version of this design will be further increased by implementing a beam steering system that is capable of tracking users.

#### **4.3.2 Angular Motion Tolerance**

In addition to variations in lateral positions, it is also important to consider variations in the incident angle of the transmitted beam relative to the optical receiver. As users move through a work space, they will naturally alter the angle of their receiver with respect to a transmitting light source. These variations have

a significant impact on the amount of received optical power. In Figure 6(b) the relationship between BER and incident angle is plotted for a data rate of 1.25 Gb/s at a range of 3 m. In the plot, the BER remains at a level of  $10^{-10}$  for angles less than 17 degrees. This result is expected because there is no optical component placed in front of the receiving photodiode, such as a lens. Therefore, changes in the incident angle have very little effect on the performance of the system. However, the photodiode is packaged in a housing where it is recessed slightly. When the incident angle exceeds 17 degrees, the packaging begins to shadow the photodiode and the BER increases. The angular tolerance in our system could easily be further improved by simply redesigning the photodiode housing so that the diode is flush with the surface of its package.

In our FSO communications system, the fact that there are no optical components concentrating light onto the receiver is very important. Optical concentrators, such as lenses and parabolic reflectors, can be powerful tools when it is necessary to increase power density; however, the penalty for using an optical concentrator is a reduction in the receiver's viewing angle and therefore a reduction in angular tolerance. The reduction in viewing angle is directly proportional to the concentration gain factor provided by the concentrating element. In point-to-point FSO systems, a single lens with an arbitrarily large diameter can be used to focus light down to a diffraction-limited spot size assuming the transmitted beam is monochromatic. Doing so, however, reduces

the viewing angle of the receiver down to a fraction of a degree, necessitating that the receiver be oriented in the exact direction of the transmitter. This configuration is simply not feasible in a scenario in which the exact position and orientation of the transmitter and receiver are not known to both components. Even if it is assumed that such information did exist, each component would require an additional mechanical stage that could align the two halves of the link.

In contrast, our design eliminates these issues by providing 500 mW of average output power. On the receiver side, the avalanche gain factor provided by the APD further reduces the need for an optical concentrator. By avoiding the use of a receiver-side optical concentrator completely, an angular tolerance of 27 degrees was achieved.

### **4.3.3 Data Throughput Evaluation**

Defining the relationship between BER and data rate is critical when evaluating the performance of a communications system. In the two previous evaluations, the data rate was fixed to 1.25 Gb/s and the BER rate was measured as a function of special parameters. In this evaluation, the receiver is placed 3 m away from the transmitter and the BER is measured as a function of data rate. The receiver is also placed on the optical axis and oriented incident normal to the transmitted beam. The results of this evaluation are plotted in Figure 6(c). For

data rates less than 1.2 Gb/s, the optical transmissions are error free. Between 1.2 Gb/s and 1.3 Gb/s the BER begins to increase rapidly, but then levels off. A maximum data rate of 1.45 Gb/s is achieved while still maintaining a BER below  $10^{-4}$ . Eye diagrams showing recovered optical signals at data rates of 1 Gb/s, 1.2 Gb/s, and 1.45 Gb/s are shown in Figure 7.

When compared to commercially available single VCSEL diode transmitters, the data rates presented in this paper are highly competitive. For example, Finisar currently markets a 2.5 Gb/s VCSEL device with a power output of 2 mW. This device is 1.7 times faster than our VCSEL array transmitter but produces 250 times less power. Although there is a slight bandwidth penalty when using a VCSEL array, the increase in power output far exceeds the reduction in bandwidth. From an FSO system design perspective, the VCSEL array device is clearly superior.

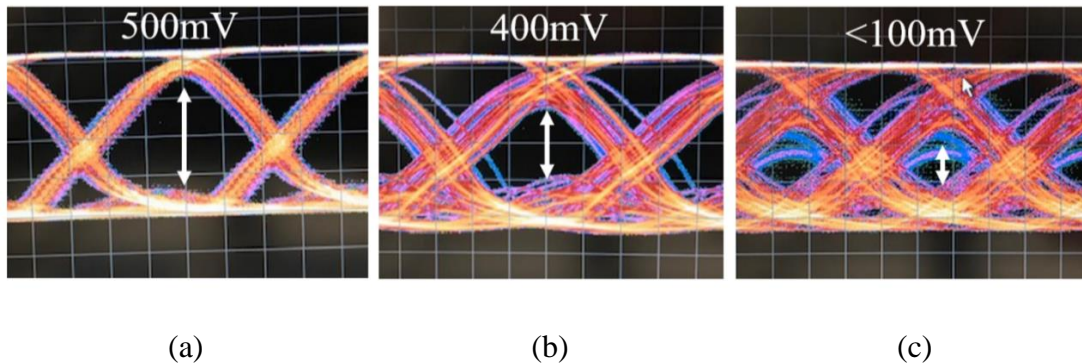
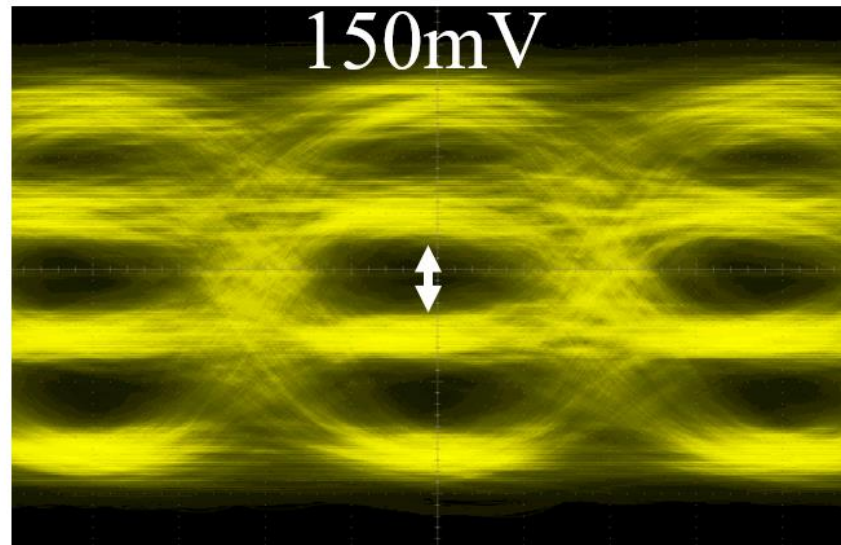


Figure 4.7: Eye diagrams showing FSO signals recovered over a 3 m optical channel – (a) 1 Gb/s, (b) 1.25 Gb/s, (c) 1.45 Gb/s

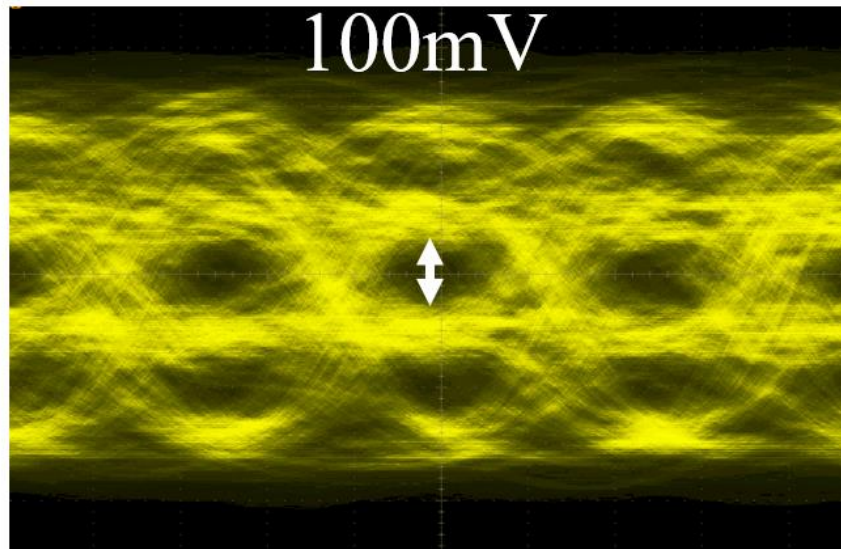
#### 4.3.4 PAM4 Modulation Symbols

In addition to OOK modulation, a higher-order PAM4 modulation scheme was also considered. PAM4 signals contain twice as much information as OOK signals but require three times the SNR. Due to the high output power of our VCSEL array transmitter, the SNR of the recovered optical signal 3 m away from the transmitter still has a sufficiently high SNR to support PAM4 signals. Therefore, a PAM4 modulation scheme might be one way in which bandwidth in our FSO communications system could be increased.

As a proof of concept, PAM4 signals were transmitted across 3 m of free space using the experimental setup described in this section. The PRBS PAM4 data signals that were used for this demonstration were generated in Matlab and then exported to an arbitrary waveform generator (AWG). The AWG was then used to drive our VCSEL array transmitter. On the receiver end, the recovered PAM4 signal was captured using an oscilloscope. The results of this demonstration are shown in Figure 8(a) and 8(b) at data rates of 1 Gb/s and 2 Gb/s respectively. At a rate of 1 Gb/s, each of the four signal levels are clearly distinguishable; however, when the data rate increases to 2 Gb/s the signal quality deteriorates significantly. This proof of concept demonstrates that the linearity of our VCSEL array transmitter is adequate for higher-order modulation schemes, although more work is required to fully utilize the potential of the PAM4 format.



(a)



(b)

Figure 4.8: Eye diagrams showing PAM4 signals recovered over a 3 m optical channel – (a) 1 Gb/s, (b) 2 Gb/s

## 4.4 Summary

In this chapter, an FSO communication system consisting of a high-power VCSEL array transmitter and a high-sensitivity receiver was presented. This 850 nm VCSEL array transmitter has a maximum throughput of 1.45 Gb/s using an OOK modulation scheme and is based on a novel distributed-current laser driver design utilizing E-pHEMT transistors. The transmitter delivers 500 mW of average optical power and can cover an area of approximately 1 m<sup>2</sup> at a distance of 3 m while still maintaining a BER <10<sup>-4</sup>. The high-sensitivity optical receiver does not require light-concentrating optics and can tolerate angular variations up to 27 degrees. In addition to OOK, a PAM4 modulation scheme was also demonstrated. This FSO communications system offers an effective and scalable solution to the limited bandwidth available in traditional RF networks.

## CHAPTER 5. CONCLUSIONS

Currently, overcrowding in the radio frequency spectrum is limiting data throughput capacity in short-range wireless networks like WiFi. Indoor free-space optical communication links offer a possible solution to this problem as an augmentation to or replacement for traditional WiFi links. Wireless links utilizing optical frequencies have attracted significant attention due to their large bandwidth potentials and line-of-sight nature. Optical frequencies represent hundreds of terahertz of unregulated spectrum, and therefore hold tremendous potential. Additionally, optical frequencies are highly directional by nature and do not penetrate through walls. The latter property creates a physical layer of protection against individuals who may wish to intercept or corrupt data transmissions. Although the line-of-sight property of optical transmissions improves security, it also poses a challenge for mobility. Mobility is central to any wireless network and represents a main advantage that wireless networks have over wireline connections. As such, any free-space optical network will need to thoroughly address the question of mobility in its design. In this dissertation, several scalable free-space optical communications systems were presented and analyzed in detail. Additionally, the question of mobility was addressed in the context of each system, with emphasis on the fundamental tradeoff between bandwidth and mobility.

The first system that we proposed was designed to deliver a cost-effective free-space optical network solution that could be quickly deployed into an office environment with very little retrofitting involved. This system utilized low-cost infrared LEDs and took a hybrid optical and radio frequency approach to ensuring mobility. The optical half of the network only provided a downlink to end users, while the uplink and mobility protocol were both handled using a WiFi network. This compromise allowed the optical portion of the network to take over the majority of the data throughput functions, while ensuring a constant wireless connection was maintained, even when users moved between optical cells. A network protocol was also developed for this system, which encapsulated all the network functions. Although this system was highly functional, data rates were restricted to 50 Mb/s.

The second proposed system presented in this dissertation was focused on laser-based optical transmitters and examined the use of overlapping optical femtocells and attocells. In this system, the diverse needs of potential users were addressed through the creation of two parallel optical cells occupying the same space. First, a femtocell based on a 980 nm side-emitting Fabry-Perot laser diode was presented with a bandwidth of 100 Mb/s and a cell diameter of 60 cm. Second, an attocell based on an 850 nm VCSEL diode was presented with a bandwidth of 1.5 Gb/s and a cell diameter of 1 cm. Each cell was designed to meet the specific bandwidth and mobility needs of users seeking access to a wireless connection.

Interference between the two links was addressed using a combination of optical and frequency filtering. An optical bandpass filter was placed in front of the attocell link to ensure that light from the femtocell was filtered out. In the femtocell link, a large-area photodiode was used but proved incapable of sensing the high-speed attocell signal. Together, these two strategies allow both links to operate simultaneously in the same space without interference. Our dual-channel femtocell and attocell link highlights that specific tradeoff that must be considered between bandwidth and mobility in any optical communication system.

The final system proposed in this dissertation examined the use of an arrayed light source as a means of achieving both high power output and high bandwidth. Specifically, we evaluated a 60-element, 500 mW, 850 nm VCSEL array. Due to the parallel wiring of the array, the device required currents of up to 1 A, making the device difficult to drive. To overcome this challenge, a distributed-current laser driver was designed and fabricated to deliver 1 A of current at gigabit-per-second speeds. With our custom-built laser driver and VCSEL array, we were able to create a 1.25 Gb/s optical femtocell with a diameter of 12 cm. Although this link does not provide a high level of mobility on its own, it does reduce the precision of alignment that is required when compared to the attocell link presented in chapter three. In future versions of the system, the transmitter will be paired with a beam steering device that will direct the optical link in the direction of a user. If extremely high precision is required to maintain the link, the system reliability will be low.

Therefore, reducing the need for precision alignment is a key step toward high-mobility, gigabit-per-second optical links.

In summary, the body of work presented in this dissertation represents an in-depth investigation into the potential of indoor free-space optical networks. We have presented several optical link prototype systems that are individually optimized for cost, mobility, and bandwidth. Each of the systems described in this dissertation are analyzed in terms of range, throughput, and bit error rate. Additionally, we have provided a network-level framework in which hybrid or standalone optical networks can operate. Our investigation has found that free-space optical networks offer a viable and attractive alternative to traditional radio-frequency networks. It is clear that as congestion in the radio-frequency band of the electromagnetic spectrum increases, optical transceivers will play a greater role in wireless networks. For enterprises concerned in maintaining a competitive edge in wireless network technology, future investment and development in the field of free-space optical communications is critical.

## References

- [1] H. Zhao *et al.*, "3 Gbps Free Space Optical Link based on Integrated Indium Phosphide Transmitter," *2018 76th Device Research Conference (DRC)*, Santa Barbara, CA, 2018, pp. 1-2.
- [2] X. Zhang *et al.*, "Free-space broad-spectrum optical communication based on supercontinuum," *2017 16th International Conference on Optical Communications and Networks (ICOCN)*, Wuzhen, 2017, pp. 1-3.
- [3] R. Mesleh and A. AL-Olaimat, "Acousto-optical modulators for free space optical wireless communication systems," in *IEEE/OSA Journal of Optical Communications and Networking*, vol. 10, no. 5, pp. 515-522, May 2018.
- [4] Z. V. Rizou, K. E. Zoiros and A. Hatziefremidis, "Signal amplitude and phase equalization technique for free space optical communications," *2013 15th International Conference on Transparent Optical Networks (ICTON)*, Cartagena, 2013, pp. 1-4.
- [5] E. Samain *et al.*, "First free space optical communication in europe between SOTA and MeO optical ground station," *2015 IEEE International Conference on Space Optical Systems and Applications (ICSOS)*, New Orleans, LA, 2015, pp. 1-7.
- [6] M. Presi, R. Corsini, M. Artiglia, F. Bottoni, G. Cossu and E. Ciaramella, "Low-cost 6.25 GHz UDWDM-PON based on direct intensity-modulated transmitters," *2015 Optical Fiber Communications Conference and Exhibition (OFC)*, Los Angeles, CA, 2015, pp. 1-3.
- [7] Spencer Liverman, Qiwei Wang, Yu-Jung Chu, Anindita Borah, Songtao Wang, Arun Natarajan, Alan X. Wang, Thinh Nguyen, "WiFO: A hybrid communication network based on integrated free-space optical and WiFi femtocells," Computer Communications, Volume 132, 2018.
- [8] Qiwei Wang, Spencer Liverman, Yu-jung Chu, Anindita Borah, Songtao Wang, Thinh Nguyen, Arun Natarajan, Alan Wang, "WiFO: A Hybrid WiFi free-Space optical communication networks of femtocells," MSWiM Conference, 35-42. 2017.
- [9] Chuanbowen Sun, S. H. Bae, H. Kim and Y. C. Chung, "Transmission of 28-Gb/s duobinary signals over 45-km SSMF Using 1.55- $\mu$ m directly modulated laser," *2016 21st OptoElectronics and Communications Conference (OECC) held jointly with 2016 International Conference on Photonics in Switching (PS)*, Niigata, 2016, pp. 1-3.
- [10] D. Schoeniger, R. Henker and F. Ellinger, "An 850-nm common-cathode VCSEL driver with tunable energy efficiency for 45 Gbit/s data transmission without equalization," *2017 IEEE Asia Pacific Microwave Conference (APMC)*, Kuala Lumpur, 2017, pp. 1103-1106.

- [11] M. Z. Afgani, H. Haas, H. Elgala, D. Knipp, "Visible light communication using ofdm," 2nd International Conference on Testbeds and Research Infrastructures for the Development of Networks and Communities., TRIDENTCOM (2006) 6–134.
- [12] M. Kavehrad, "Sustainable energy-efficient wireless applications using light," *IEEE Communication Magazine* (2010) 66–73
- [13] K. Wang, A. Nirmalathas, C. Lim, and E. Skafidas, "Ultra-broadband indoor optical wireless communication system with multimode fiber," *Optics Letters*, 37, 2012, 1514–1516.
- [14] C. Kottke, J. Hilt, K. Habel, J. Vučić, K.-D. Langer, "1.25 gbit/s visible light wdm link based on dmt modulation of a single rgb led luminary," European Conference and Exhibition on Optical Communication, p. We.3.B.4, Optical Society of America, 2012.
- [15] Y. Wang, Y. Wang, N. Chi, J. Yu, H. Shang, "Demonstration of 575- mb/s downlink and 225-mb/s uplink bi-directional scm-wdm visible light communication using rgb led and phosphor-based led," *Opt. Express*, vol. 21, pp. 1203–1208, 2013.
- [16] J. McKendry, D. Massoubre, S. Zhang, B. Rae, R. Green, E. Gu, R. Henderson, A. Kelly, M. Dawson, "Visible-light communications using a cmos-controlled micro-light- emitting-diode array," *Journal of Lightwave Technology*, vol. 30, pp. 61–67, 2012.
- [17] Y. Zhao and C. Shu, "Wavelength tunable single-mode oscillation of a gain-switched FP laser diode with repetition rate from 89 MHz to 1.02 GHz by self-injection seeding with a fiber grating," *Conference Proceedings. LEOS '97. 10th Annual Meeting IEEE Lasers and Electro-Optics Society 1997 Annual Meeting*, San Francisco, CA, USA, 1997, pp. 221-222 vol.2.
- [18] C. Lee *et al.*, "High speed performance of III-nitride laser diode grown on (2021) semipolar plane for visible light communication," *2016 IEEE Photonics Conference (IPC)*, Waikoloa, HI, 2016, pp. 809-810.
- [19] T. Wu *et al.*, "White-Lighting Communication With a Lu<sub>3</sub>Al<sub>5</sub>O<sub>12</sub>:Ce<sup>3+</sup>/CaAlSiN<sub>3</sub>:Eu<sup>2+</sup> Glass Covered 450-nm InGaN Laser Diode," in *Journal of Lightwave Technology*, vol. 36, no. 9, pp. 1634-1643, 1 May1, 2018.
- [20] J. J. Huang *et al.*, "Manufacturing excellence and future challenges of wireless laser components for 4G/5G optical mobile fronthaul networks," *2018 27th Wireless and Optical Communication Conference (WOCC)*, Hualien, 2018, pp. 1-2.
- [21] S. T. M. Fryslie, A. Netherton, N. DeNardo, H. Dave, K. Lakomy and K. D. Choquette, "Aspects of direct modulation of VCSELs," *2016*

- International Semiconductor Laser Conference (ISLC)*, Kobe, 2016, pp. 1-2
- [22] M. Hirota, S. Iio, Y. Ohta, Y. Niwa and T. Miyamoto, "Wireless power transmission between a NIR VCSEL array and silicon solar cells," *2015 20th Microoptics Conference (MOC)*, Fukuoka, 2015, pp. 1-2.
- [23] R. Safaisini, J. R. Joseph and K. L. Lear, "Scalable High-CW-Power High-Speed 980-nm VCSEL Arrays," in *IEEE Journal of Quantum Electronics*, vol. 46, no. 11, pp. 1590-1596, Nov. 2010.
- [24] W. Hofmann, E. Wong, G. Bohm, M. Ortsiefer, N. H. Zhu and M. C. Amann, "1.55 $\mu$ m VCSEL Arrays for High-Bandwidth WDM-PONs," in *IEEE Photonics Technology Letters*, vol. 20, no. 4, pp. 291-293, Feb. 15, 2008.
- [25] S. Spiga, C. Xie, P. Dong, M. C. Amann and P. Winzer, "Ultra-high-bandwidth monolithic VCSEL arrays for high-speed metro networks," *2014 16th International Conference on Transparent Optical Networks (ICTON)*, Graz, 2014, pp. 1-4
- [26] W. S. Oh and K. Park, "Design of a 4-channel 10-Gb/s CMOS VCSEL driver array," *2008 7th International Conference on Optical Internet*, Tokyo, 2008, pp. 1-2.
- [27] L. Zhang, H. Chun, G. Faulkner, D. O'Brien and S. Collins, "Efficient pulse amplitude modulation for SPAD-based receivers," *2018 Global LiFi Congress (GLC)*, Paris, 2018, pp. 1-5.
- [28] E. Bialic, "Semi-transparent solar cells indifferent to ambient lighting for LiFi application," *2016 IEEE International Conference on Wireless for Space and Extreme Environments (WiSEE)*, Aachen, 2016, pp. 37-41
- [29] X. Li, B. Hussain, L. Wang, J. Jiang and C. P. Yue, "A 2.2-mW 24-Mb/s CMOS LiFi receiver system-on-a-chip with ambient light rejection and post-equalization," *2017 IEEE Photonics Conference (IPC)*, Orlando, FL, 2017, pp. 29-30.
- [30] B. Fahs, A. J. Chowdhury, J. Ghasemi, P. Zarkesh-Ha and M. M. Hella, "A robust 2 $\times$ 2 CMOS receiver array for meter-scale point-to-point OOK VLC links," *2017 IEEE 60th International Midwest Symposium on Circuits and Systems (MWSCAS)*, Boston, MA, 2017, pp. 663-666.
- [30] Cisco Visual Networking Index, Available: <http://www.cisco.com/c/en/us/solutions/collateral/service-provider/visual-networking-index-vni/complete-white-paper-c11-481360.html>, 2016.
- [31] FC Spectrum Policy Task Force, Report of the spectrum efficiency working group, Available: <http://www.fcc.gov/sptf/reports.html>
- [32] Qin Zhao, B.M. Sadler, "A survey of dynamic spectrum access," *Signal Processing Magazine*, IEEE 24, 2007, 79 –89.

- [33] J. Mitola III, G.Q. Maguire Jr., "Cognitive radio: making software radios more personal," *Personal Communications*, IEEE 6, 4 (1999), 13–18.
- [34] A. T. Hussein, J. M. H. Elmirghani, "Mobile multi-gigabit visible light communication system in realistic indoor environment," *Journal of Lightwave Technology*, vol. 33, pp. 3293–3307, 2015.
- [35] I. Stefan, H. Haas, "Hybrid visible light and radio frequency communication systems," IEEE 80th Vehicular Technology Conference., pp. 1–5, 2014.
- [36] S. Bloom and W. Hartley, The last-mile solution: hybrid FSO radio. AirFiber Inc., May 2002.
- [37] H. Wu, B. Hamzeh, and M. Kavehrad, "Achieving carrier class availability of fso link via a complementary rf link," in Signals, Systems and Computers, 2004. Conference Record of the Thirty-Eighth Asilomar Conference on, vol. 2, pp. 1483–1487 Vol.2, Nov 2004.
- [38] A. Abdulhussein, A. Oka, T. T. Nguyen and L. Lampe, "Rateless coding for hybrid free-space optical and radio-frequency communication," in Wireless Communications, IEEE Transactions, vol. 9, pp. 907-913, Mar. 2010.
- [39] D. Wang and A. Abouzeid, "Throughput capacity of hybrid radio-frequency and free-space-optical (rf/fs) multi-hop networks," in Information Theory and Applications Workshop, 2007, pp. 3-10, Jan. 2007.
- [40] A. Eslami, S. Vangala and H. Pishro-Nik, "Hybrid channel codes for efficient fso/rf communication systems," in Communications, IEEE Transactions, vol. 58, pp. 2926-2938, Oct. 2010.
- [41] Y. Tang, M. Brandt-Pearce and S. Wilson, "Link adaptation for throughput optimization of parallel channels with application to hybrid fso/rf systems," in Communications, IEEE Transactions, vol. 60, pp. 2723-2732, Sep. 2012.
- [42] F. Ahdi and S. Subramaniam, "Optimal placement of fso links in hybrid wireless optical networks," in Global Telecommunications Conference (GLOBECOM 2011), 2011 IEEE, pp. 1-6, Dec. 2011.
- [43] N. Letzepis, K. Nguyen, A. Guillen Fabregas and W. Cowley, "Outage analysis of the hybrid free-space optical and radio-frequency channel," in Selected Areas in Communications, IEEE Journal, vol. 27, pp. 1709-1719, Dec. 2009.
- [44] H. Al Hajjar, B. Fracasso, and D. LerouxIndoor, "Optical wireless Gbps link dimensioning," National Fiber Optic Engineers Conference, Anaheim, CA (2013) 17-21.
- [45] G. Cossu, A. M. Khalid, P. Choudhury, R. Corsini, E. Ciaramella, "2.1 gbit/s visible optical wireless transmission," European Conference and Exhibition on Optical Communication, p. P4.16, Optical Society of America, 2012.
- [46] Y. Zheng, M. Zhang, "Visible light communications-recent progresses and future outlooks," Photonics and Optoelectronic (SOP) Symposium, pp. 1–

- 6, 2010.
- [47] W. O. Popoola, "Impact of vlc on light emission quality of white leds," *Journal of Lightwave Technology*, vol. 34, pp. 2526–2532, 2016.
- [48] H. L. Minh, D. O'Brien, G. Faulkner, L. Zeng, K. Lee, D. Jung, Y. Oh, "80 mbit/s visible light communications using pre-equalized white led," Optical Communication 34th European Conference, pp. 1–2, 2008.
- [49] L. Grobe, A. Paraskevopoulos, J. Hilt, D. Schulz, F. Lassak, F. Hartlieb, C. Kottke, V. Jungnickel, K.-D. Langer, "High speed visible light communication systems," *Communications Magazine*, IEEE, vol. 51, pp. 60–66, 2013.
- [50] J. Vucic, C. Kottke, S. Nerreter, K.-D. Langer, J. Walewski, "513 mbit/s visible light communications link based on dmt-modulation of a white led," *Journal of Lightwave Technology*, vol. 28, pp. 3512–3518, 2010.
- [51] A. Khalid, G. Cossu, R. Corsini, P. Choudhury, E. Ciaramella, "1-gb/s transmission over a phosphorescent white led by using rateadaptive discrete multitone modulation," *IEEE Photonics Journal*, vol. 4, pp. 1465–1473, 2012.
- [52] Krzysztof Szczerba, Petter Westbergh, Johnny Karout, Johan S. Gustavsson, Asa Haglund, Magnus Karlsson, Peter A. Andrekson, Erik Agrell, Anders Larsson, "4-pam for high-speed short-range optical communications," *Journal of Optical Communications and Networking*, Volume 4, No. 11, 2012.
- [53] Moshe Medina, David Kin, Alex Shar, Yishai Gourman, Ariel Carmeli, Slava Krylov, "Micro mirrors for MEMS based free space point to point indoor wireless optical network (IWON)," IEEE International Conference on Optical MEMS and Nanophotonics, 2-5, 2015.
- [54] Huanhuan Zheng, Zhaowen Xu, Changyuan Yu, Mohan Gurusamy, "A 3-D high accuracy positioning system based on visible light communication with novel positioning algorithm," *Optics Communications*, Volume 396, 2017.
- [55] A. Burton, E. Bentley, H. L. Minh, Z. Ghassemlooy, N. Aslam, S.-K. Liaw, "Experimental demonstration of a 10base-t ethernet visible light communications system using white phosphor light-emitting diodes," *Circuits, Devices Systems*, IET, vol. 8, pp. 322–330, 2014.
- [56] S. Liverman, Q. Wang, Y. Chu, T. Duong, D. Nyuyen-Huu, S. Wang, T. Nguyen, A. X. Wang, "Integrating free-space optical communication links with existing wifi (wifo) network," SPIE Photonics West, pp. 97720P–97720P, 2015.
- [57] H. Elgala, R. Mesleh, H. Haas, "Indoor optical wireless communication: potential and state-of-the-art," *IEEE Communications Magazine*, vol. 49, pp. 56–62, 2011.

- [58] Di Wang and Alhussein A. Abouzeid, "Throughput and Delay Analysis for Hybrid Radio-frequency and Free-space-optical (RF/FSO) Networks," *Wirel. Netw.* 17 (2011), 877–892.
- [59] O. Bouchet, M. El Tabach, M. Wolf, D. O'brien, G. Faulkner, J.W. Walewski, S. Randel, M. Franke, S. Nerreter, K.-D. Langer, J. Grubor, and T. Kamalakis, "Hybrid wireless optics (HWO): Building the next-generation home network," CNSDSP (2008) 283–287.
- [60] Y. Wang, X. Wu, and H. Haas, "Distributed load balancing for Internet of Things by using Li Fi and RF hybrid network," IEEE 26th Annual International Symposium on Personal, Indoor, and Mobile Radio Communications (2015) 1289–1294.
- [61] H. Haas, L. Yin, Y. Wang, C. Chen, "What is lifi?," *Journal of Lightwave Technology*, vol. 34, pp. 1533–1544, 2016.
- [62] Hao Ma, Lutz Lampe, Steve Hranilovic, "Hybrid visible light and power line communication for indoor multiuser downlink," *Journal of Optical Communications and Networking*, Volume 9, No. 8, 2017.
- [63] Q. Wang, T. Nguyen, A. X. Wang, "Channel capacity optimization for an integrated wi-fi and free-space communication system (wififo)," Proceedings of the 17th ACM international conference on Modeling, analysis and simulation of wireless and mobile systems, pp. 327-330, 2014.
- [64] J. Wang, C. Jiang, H. Zhang, X. Zhang, V. C. M. Leung and L. Hanzo, "Learning-Aided Network Association for Hybrid Indoor LiFi-WiFi Systems," in *IEEE Transactions on Vehicular Technology*, vol. 67, no. 4, pp. 3561-3574, April 2018.
- [65] X. Wu, M. Safari and H. Haas, "Access Point Selection for Hybrid Li-Fi and Wi-Fi Networks," in *IEEE Transactions on Communications*, vol. 65, no. 12, pp. 5375-5385, Dec. 2017.
- [66] H. Alshaer and H. Haas, "Bidirectional LiFi Attocell Access Point Slicing Scheme," in *IEEE Transactions on Network and Service Management*.
- [67] T. Kishi, H. Tanaka, Y. Umeda, O. Takyu, "A high-speed led driver that sweeps out the remaining carriers for visible light communications," *Journal of Lightwave Technology*, vol. 32, pp. 239–249, 2014.
- [68] Yu-Jung Chu, "Mobility protocol, channel estimation and modulation techniques for hybrid wifi-fso (wifo) wlan of femtocells," *Thesis (M.S.)*, *Degree Granting Institute*, Oregon State University, 2016.
- [69] L. Feng, R. Q. Hu, J. Wang, P. Xu and Y. Qian, "Applying VLC in 5G Networks: Architectures and Key Technologies," in *IEEE Network*, vol. 30, no. 6, pp. 77-83, November-December 2016.
- [70] A. Gupta, P. Garg and N. Sharma, "Hybrid LiFi — WiFi indoor broadcasting system," *2017 IEEE 28th Annual International Symposium on Personal, Indoor, and Mobile Radio Communications (PIMRC)*, Montreal,

- QC, 2017, pp. 1-6.
- [71] D. Singh, A. Sood, G. Thakur, N. Arora and A. Kumar, "Design and implementation of wireless communication system for toll collection using LiFi," *2017 4th International Conference on Signal Processing, Computing and Control (ISPCC)*, Solan, 2017, pp. 510-515.
- [72] J. O. Agyemang, J. J. Kponyo and J. Mouzna, "Light Fidelity(LiFi) as an Alternative Data Transmission Medium in VANET," *2017 European Modelling Symposium (EMS)*, Manchester, United Kingdom, 2017, pp. 213-217.
- [73] A. Surampudi, S. S. Chapalgaonkar and P. Arumugam, "Can balloons produce Li-Fi? A disaster management perspective," *2018 Global LiFi Congress (GLC)*, Paris, 2018, pp. 1-5.
- [74] C. Chen, D. A. Basnayaka and H. Haas, "Downlink Performance of Optical Attocell Networks," in *Journal of Lightwave Technology*, vol. 34, no. 1, pp. 137-156, Jan.1, 1 2016.
- [75] Z. Chen and H. Haas, "Physical layer security for optical attocell networks," *2017 IEEE International Conference on Communications (ICC)*, Paris, 2017, pp. 1-6.
- [76] Z. Chen and H. Haas, "A simplified model for indoor optical attocell networks," *2015 IEEE Summer Topicals Meeting Series (SUM)*, Nassau, 2015, pp. 167-168.
- [77] K. Zhou, C. Gong and Z. Xu, "Color Planning and Intercell Interference Coordination for Multicolor Visible Light Communication Networks," in *Journal of Lightwave Technology*, vol. 35, no. 22, pp. 4980-4993, Nov.15, 15 2017.
- [78] C. Chen, D. Tsonev and H. Haas, "Joint transmission in indoor visible light communication downlink cellular networks," *2013 IEEE Globecom Workshops (GC Wkshps)*, Atlanta, GA, 2013, pp. 1127-1132.
- [79] I. S. Ansari, M. M. Abdallah, M. S. Alouini and K. A. Qaraqe, "A performance study of two hop transmission in mixed underlay RF and FSO fading channels," *2014 IEEE Wireless Communications and Networking Conference (WCNC)*, Istanbul, 2014, pp. 388-393.
- [80] I. S. Ansari, M. M. Abdallah, M. S. Alouini and K. A. Qaraqe, "Outage performance analysis of underlay cognitive RF and FSO wireless channels," *2014 3rd International Workshop in Optical Wireless Communications (IWOW)*, Funchal, 2014, pp. 6-10.
- [81] M. D. Soltani, H. Kazemi, M. Safari and H. Haas, "Handover Modeling for Indoor Li-Fi Cellular Networks: The Effects of Receiver Mobility and Rotation," *2017 IEEE Wireless Communications and Networking Conference (WCNC)*, San Francisco, CA, 2017, pp. 1-6.
- [82] Y. Wang, X. Wu and H. Haas, "Fuzzy logic based dynamic handover

- scheme for indoor Li-Fi and RF hybrid network," *2016 IEEE International Conference on Communications (ICC)*, Kuala Lumpur, 2016, pp. 1-6.
- [83] Y. Wang and H. Haas, "Dynamic load balancing with handover in hybrid li-fi and wi-fi networks," in *Journal of Lightwave Technology*, vol. 33, no. 22, pp. 4671-4682, Nov.15, 15 2015.
- [84] D. Nguyen-Huu, T. Duong and T. Nguyen, "Location-Assisted Coding for FSO Communication," in *IEEE Transactions on Communications*, vol. 65, no. 10, pp. 4360-4370, Oct. 2017.
- [85] M. D. Soltani, X. Wu, M. Safari and H. Haas, "Bidirectional User Throughput Maximization Based on Feedback Reduction in LiFi Networks," in *IEEE Transactions on Communications*.
- [86] Z. Chen, D. A. Basnayaka and H. Haas, "Space Division Multiple Access for Optical Attocell Network Using Angle Diversity Transmitters," in *Journal of Lightwave Technology*, vol. 35, no. 11, pp. 2118-2131, June1, 1 2017.
- [87] Z. Chen, D. A. Basnayaka and H. Haas, "Space division multiple access in optical attocell networks," *2016 IEEE Wireless Communications and Networking Conference*, Doha, 2016, pp. 1-5.
- [88] Z. P. Choudhari and S. R. Devane, "High sensitivity universal lifi receiver for enhance data communication," *2016 Online International Conference on Green Engineering and Technologies (IC-GET)*, Coimbatore, 2016, pp. 1-5.
- [89] K. C. Hu, A. G. Armada, M. Sánchez-Fernández and A. Royo, "Prototyping and measurements for a LiFi system," *2016 IEEE Sensor Array and Multichannel Signal Processing Workshop (SAM)*, Rio de Janerio, 2016, pp. 1-5.
- [90] N. Lorrière *et al.*, "An OFDM testbed for LiFi performance characterization of photovoltaic modules," *2018 Global LIFI Congress (GLC)*, Paris, 2018, pp. 1-5.
- [91] M. R. H. Mondal and R. B. Faruque, "Hybrid diversity combined OFDM for LiFi," *2017 IEEE International Conference on Telecommunications and Photonics (ICTP)*, Dhaka, 2017, pp. 132-136.
- [92] H. Kazemi, M. Safari and H. Haas, "A wireless backhaul solution using visible light communication for indoor Li-Fi attocell networks," *2017 IEEE International Conference on Communications (ICC)*, Paris, 2017, pp. 1-7.
- [93] H. Kazemi, M. Safari and H. Haas, "Spectral Efficient Cooperative Downlink Transmission Schemes for DCO-OFDM-Based Optical Attocell Networks," *2016 IEEE 84th Vehicular Technology Conference (VTC-Fall)*, Montreal, QC, 2016, pp. 1-6.
- [94] Spencer Liverman, Qiwei Wang, Yu-Jung Chu, Anindita Borah, Songtao Wang, Arun Natarajan, Alan X. Wang, Thinh Nguyen, "WiFO: A hybrid

- communication network based on integrated free-space optical and WiFi femtocells," *Computer Communications*, Volume 132, 2018.
- [95] M. Zeng, K. Zhou, C. Gong, S. Lou, X. Jin and Z. Xu, "Design and demonstration of an indoor visible light communication network with dynamic user access and resource allocation," *2017 9th International Conference on Wireless Communications and Signal Processing (WCSP)*, Nanjing, 2017, pp. 1-6.
- [96] Liya Yi and Tao Cui, "Interference mitigation between femtocell and macrocell," *Proceedings of 2011 International Conference on Electronics and Optoelectronics*, Dalian, Liaoning, 2011, pp. V2-102-V2-104.
- [97] H. Kazemi and H. Haas, "Downlink cooperation with fractional frequency reuse in DCO-OFDMA optical attocell networks," *2016 IEEE International Conference on Communications (ICC)*, Kuala Lumpur, 2016, pp. 1-6.
- [98] C. Chen, D. Basnayaka and H. Haas, "Downlink SINR Statistics in OFDM-Based Optical Attocell Networks with a Poisson Point Process Network Model," *2015 IEEE Global Communications Conference (GLOBECOM)*, San Diego, CA, 2015, pp. 1-6.
- [99] A. Rissons, J. Perchoux and J. C. Mollier, "Small signal and noise circuit model of vertical-cavity surface-emitting laser (VCSEL) arrays for short range optomicrowave links," *MWP 2003 Proceedings. International Topical Meeting on Microwave Photonics*, 2003., 2003, pp. 211-214.
- [100] A. Al-Omari G. P. Carey S. Hallstein J. P. Watson G. Dang and K. L. Lear "Low thermal resistance high speed top emitting 980nm VCSELs " *Photonics Technology Letters* vol. 18 pp. 1225-1227 June 2006.
- [101] R. Amatya, D. Luerssen, M. Farzaneh and J. A. Hudgins, "Thermal lensing in oxide-confined, single-mode VCSELs," *2006 Conference on Lasers and Electro-Optics and 2006 Quantum Electronics and Laser Science Conference*, Long Beach, CA, 2006, pp. 1-2.
- [102] R. Amatya, D. Luerssen, M. Farzaneh and J. A. Hudgins, "Thermal lensing in oxide-confined, single-mode VCSELs," *2006 Conference on Lasers and Electro-Optics and 2006 Quantum Electronics and Laser Science Conference*, Long Beach, CA, 2006, pp. 1-2.
- [103] W. Hofmann, M. Gorblich, M. Ortsiefer, G. Bohm and M. C. Amann, "Long-wavelength ( $\lambda = 1.55\mu\text{m}$ ) monolithic VCSEL array with > 3W CW output power," in *Electronics Letters*, vol. 43, no. 19, pp. 1025-1026, September 13 2007.
- [104] M. Hirota, S. Iio, Y. Ohta, Y. Niwa and T. Miyamoto, "Wireless power transmission between a NIR VCSEL array and silicon solar cells," *2015 20th Microoptics Conference (MOC)*, Fukuoka, 2015, pp. 1-2.

- [105] Y. Katsuta and T. Miyamoto, "Efficiency improvement by serial-connection of VCSEL array for optical wireless power transmission," *2017 22nd Microoptics Conference (MOC)*, Tokyo, 2017.
- [106] "Strength in numbers," in *Electronics Letters*, vol. 46, no. 10, pp. 667-667, 13 May 2010.
- [107] H. Roscher and R. Michalzik, "Low thermal resistance flip-chip bonding of 850 nm 2-D VCSEL arrays capable of 10 Gbps operation," *The 16th Annual Meeting of the IEEE Lasers and Electro-Optics Society, 2003. LEOS 2003.*, 2003, pp. 511-512 vol.2
- [108] R. Safaisini, J. R. Joseph and K. L. Lear, "Scalable High-CW-Power High-Speed 980-nm VCSEL Arrays," in *IEEE Journal of Quantum Electronics*, vol. 46, no. 11, pp. 1590-1596, Nov. 2010.
- [109] R. Safaisini, J. R. Joseph, G. Dang and K. L. Lear, "Uniform high bandwidth, high CW power VCSEL arrays," *2009 Conference on Lasers and Electro-Optics and 2009 Conference on Quantum electronics and Laser Science Conference*, Baltimore, MD, 2009, pp. 1-2.
- [110] M. Yoshikawa, A. Murakami, J. Sakurai, H. Nakayama and T. Nakamura, "High power VCSEL devices for free space optical communications," *Proceedings Electronic Components and Technology, 2005. ECTC '05.*, Lake Buena Vista, FL, 2005, pp. 1353-1358 Vol. 2.
- [111] Q. Wang, S. Liverman, Y. Chu, A. Borah, S. Wang, T. Nguyen, A. Natarajan, and A. X. Wang. 2017, "WiFO: a hybrid wifi free-space optical communication networks of femtocells,". In *Proceedings of the 20th ACM International Conference on Modelling, Analysis and Simulation of Wireless and Mobile Systems*, 2017.
- [112] S. Liverman, Q. Wang, Y. Chu, A. Natarajan, T. Nguyen, and A. X. Wang, "Hybrid wireless communication networks: integrating free-space optics and wifi," in *Frontiers in Optics 2016*, OSA Technical Digest, Optical Society of America, 2016.
- [113] S. Liverman, Q. Wang, Y. Chu, A. Borah, S. Wang, A. Natarajan, T. Nguyen, A. X. Wang, "Indoor communication networks realized through hybrid free-space optical and wi-fi links," Proc. SPIE 10559, Broadband Access Communication Technologies XII, 105590H, January 29 2018.
- [114] W. Hofmann, E. Wong, G. Bohm, M. Ortsiefer, N. H. Zhu and M. C. Amann, "1.55 $\mu$ m VCSEL Arrays for High-Bandwidth WDM-PONs," in *IEEE Photonics Technology Letters*, vol. 20, no. 4, pp. 291-293, Feb.15, 2008.
- [115] W. Hofmann, E. Wong, G. Bhm, M. Ortsiefer and M. C. Amann, "1 x 12 VCSEL Array at 1.55 $\mu$ m for High-Bandwidth at Metro-Range," *33rd European Conference and Exhibition of Optical Communication*, Berlin, Germany, 2007, pp. 1-2.

- [116] P. Westbergh, J. S. Gustavsson and A. Larsson, "240 Gbit/s VCSEL array for multicore fiber interconnects," *2014 IEEE Photonics Conference*, San Diego, CA, 2014, pp. 91-92.
- [117] C. W. Chow, L. Xu, C. H. Yeh, H. K. Tsang, W. Hofmann and M. C. Amann, "40-Gb/s Upstream Transmitters Using Directly Modulated 1.55- $\mu$ m VCSEL Array for High-Split-Ratio PONs," in *IEEE Photonics Technology Letters*, vol. 22, no. 5, pp. 347-349, March1, 2010.
- [118] C. Xie *et al.*, "400-Gb/s PDM-4PAM WDM System Using a Monolithic 2 $\times$ 4 VCSEL Array and Coherent Detection," in *Journal of Lightwave Technology*, vol. 33, no. 3, pp. 670-677, Feb.1, 1 2015.
- [119] S. Spiga, C. Xie, P. Dong, M. C. Amann and P. Winzer, "Ultra-high-bandwidth monolithic VCSEL arrays for high-speed metro networks," *2014 16th International Conference on Transparent Optical Networks (ICTON)*, Graz, 2014, pp. 1-4
- [120] X. Xiao *et al.*, "High-speed IQ modulator based on injection-locked VCSEL array," *2017 Conference on Lasers and Electro-Optics (CLEO)*, San Jose, CA, 2017, pp. 1-2.
- [121] I. Lu, C. Yeh, D. Hsu and C. Chow, "Utilization of 1-GHz VCSEL for 11.1-Gbps OFDM VLC Wireless Communication," in *IEEE Photonics Journal*, vol. 8, no. 3, pp. 1-6, June 2016, Art no. 7904106.
- [122] W. Hofmann, M. Gorblich, G. Bohm, M. Ortsiefer and M. C. Amann, "Long-wavelength VCSEL arrays with partly coherent emission," *2009 Conference on Lasers and Electro-Optics and 2009 Conference on Quantum electronics and Laser Science Conference*, Baltimore, MD, 2009, pp. 1-2.
- [123] M. Xun *et al.*, "High-power in-phase coherently coupled VCSEL array based on proton implantation," in *Electronics Letters*, vol. 50, no. 15, pp. 1085-1086, July 17 2014.
- [124] G. Pan *et al.*, "Large-Scale Proton-Implant-Defined VCSEL Arrays With Narrow Beamwidth," in *IEEE Electron Device Letters*, vol. 39, no. 3, pp. 390-393, March 2018.
- [125] W. S. Oh and K. Park, "Design of a 4-channel 10-Gb/s CMOS VCSEL driver array," *2008 7th International Conference on Optical Internet*, Tokyo, 2008, pp. 1-2.
- [126] Z. Zeng *et al.*, "A Compact Low-Power Driver Array for VCSELs in 65-nm CMOS Technology," in *IEEE Transactions on Nuclear Science*, vol. 64, no. 6, pp. 1599-1604, June 2017.
- [127] Won-Seok Oh, Kang-Yeob Park and Seonyoung Lee, "A 4-CH 10-Gb/s CMOS VCSEL driver array with adaptive optical power control," *2010 The 12th International Conference on Advanced Communication Technology (ICACT)*, Phoenix Park, 2010, pp. 826-829.

- [128] K. K. Gan *et al.*, "10 Gb/s radiation-hard VCSEL array driver," *2014 IEEE Nuclear Science Symposium and Medical Imaging Conference (NSS/MIC)*, Seattle, WA, 2014, pp. 1-4.
- [129] A. Malacarne *et al.*, "Optical Transmitter Based on a 1.3- $\mu$ m VCSEL and a SiGe Driver Circuit for Short-Reach Applications and Beyond," in *Journal of Lightwave Technology*, vol. 36, no. 9, pp. 1527-1536, 1 May1, 2018.
- [130] C. Kottke, J. Hilt, K. Habel, J. Vučić, K.-D. Langer, "1.25 gbit/s visible light wdm link based on dmt modulation of a single rgb led luminary," *European Conference and Exhibition on Optical Communication*, p. We.3.B.4, Optical Society of America., 2012.
- [131] C. D. Muñoz, K. Elayoubi, A. Rissóns, S. Villamizar and M. Varón, "O-band and C-band VCSEL based optoelectronic oscillator (VBO) for 1.25 Gbit/s pulsed RZ-OOK and RZ-DPSK free space optical transmissions," *2017 International Topical Meeting on Microwave Photonics (MWP)*, Beijing, 2017, pp. 1-4.